TECHNO-ECONOMIC ANALYSIS OF GREEN HYDROGEN STORAGE AND TRANSPORTATION PATHWAYS

by

Parimal KOGEKAR

TECHNO-ECONOMIC ANALYSIS OF GREEN HYDROGEN STORAGE AND TRANSPORTATION PATHWAYS

by

Parimal KOGEKAR

to obtain the degree of Master of Science in Sustainable Energy Technology
at the Delft University of Technology,
to be defended publicly on Tuesday, August 1, 2023 at 14:00 Hrs.

Student number:	5260302	
Project duration:	December 12, 2022 – August 1, 2023	
Thesis committee:	Dr. Fokko Mulder	Chair, TU Delft
	Dr. Ana Somoza Tornos	Supervisor, TU Delft
	Shahab Nazari	Supervisor, McDermott

An electronic version of this thesis is available at http://repository.tudelft.nl/.

ACKNOWLEDGEMENTS

I would like to express my heartfelt gratitude and appreciation to all those who have contributed to the successful completion of my thesis journey. This endeavor would not have been possible without the unwavering support, guidance, and encouragement from various individuals.

First and foremost, I extend my sincere thanks to TU Delft university and McDermott for providing me with the opportunity to conduct my research in collaboration with their esteemed organizations. The insights and resources they offered were invaluable in shaping the outcome of this thesis.

I am deeply indebted to my university supervisor, Prof. Dr. Ana Somoza-Tornos, for her expertise, constant encouragement, and invaluable feedback throughout the duration of this project. Her mentorship played a pivotal role in refining my ideas and improving the overall quality of my work.

I extend my profound gratitude to my company supervisors, Shahab Nazari and Alba Gonzalez Oanes from McDermott, for their guidance and support during my time at the company. Their practical insights and expertise in the field have been instrumental in my thesis journey.

To my beloved parents, and sister, who have been a constant source of love, encouragement, and motivation throughout my academic journey, I offer my deepest gratitude. Their unwavering belief in me has been the driving force behind my accomplishments, and I am forever grateful for their sacrifices and support.

To my dear friends in the Netherlands, and back in India, who have been a pillar of strength and a source of joy, I extend my warmest thanks. Your unwavering friendship has made this journey enjoyable and memorable.

Lastly, I would like to thank all those who might not be explicitly mentioned here but have contributed in various ways to this thesis and my personal growth. Your presence in my life has made a significant difference, and I am grateful for your support.

I want to express my heartfelt thanks to each one of you for being an integral part of my academic and personal journey. Your unwavering support and encouragement have played a pivotal role in making this thesis a reality.

Parimal Kogekar
Delft, July 2023

ABSTRACT

To mitigate climate change and achieve global greenhouse gas emission targets, a great deal of effort is taking place in developing low-carbon solutions in the energy sector. Energy storage technologies are expected to play a crucial role in ensuring energy security by complementing intermittent renewable energy technologies. Green hydrogen is viewed as a promising energy storage solution considering its versatility. However, the lower volumetric energy density at ambient conditions is one of the drawbacks of hydrogen when its storage and transportation are considered. To tackle this problem, multiple promising options are reviewed in this study. This report examines the physical transportation of hydrogen in the form of compressed gas and liquified hydrogen, as well as the storage and transportation of it in chemical form. The latter category includes hydrogen carriers, such as green methanol, green ammonia, and LOHCs. Physical and chemical properties of the said hydrogen vectors, their dehydrogenation and the hydrogenation processes, as well as assumptions related to transportation are investigated in this report. Moreover, different international transportation routes for the import and export of the hydrogen are considered. The UniSim Design R471 program is used to simulate the hydrogenation and dehydrogenation of the hydrogen vectors in order to determine the precise energy consumption, raw material needs, carrier production rate, etc. The total capital investment cost for each vector is calculated based on the simulations. A MATLAB model is built using the information from the literature research, the outcomes of the UniSim simulations, and the findings of the economic analysis. The MATLAB model's objective is to determine the LCOH for each hydrogen carrier supply chain. The model's finding show that supply networks using compressed hydrogen gas have the highest LCOH, whereas ammonia chains have the lowest LCOH, making them the most economical option. CO_2 emission analysis showed that toluene - MCH chain have the highest CO_2 emissions. However, both the LCOH and CO_2 emissions can be significantly reduced by electrification of the dehydrogenation process.

NOMENCLATURE

A	Equilibrium coefficient
AACE	Association for the Advancement of Cost Estimation
ASU	Air Separation Unit
B	Equilibrium coefficient
CAPEX	Capital Expenditure
CEPCI	Chemical Engineering Plant Cost Index
CGH_2	Compressed hydrogen gas
CRF	Capital Recovery Factor
CRI	Carbon Recycling International
CW	Cooling Water
D&E	Design and engineering
DBT	Dibenzyl toluene
Dis	Discharge
E_a	Activation energy
EJ	Exajoule
f_c	Factor for civil engineering
f_{el}	Factor for electrical engineering
f_{er}	Factor for equipment erection
f_i	Factor for instrumentation
f_l	Factor for lagging and painting
f_p	Factor for piping
f_s	Factor for structures and buildings
GW	Gigawatt
h	Hours
HDSAM	Hydrogen Delivery Scenario Analysis Model
i	Discount rate
in	inches
IRENA	International Renewable Energy Agency
ISBL	Inside battery limits
isen	Isentropic
JT	Joule Thomson
k	Polytropic coefficient
K_a	Equilibrium rate constant
L	liter
LCOE	Levelized Cost of Electricity

LCOH	Levelized cost of hydrogen
LGC	Large Gas Carriers
LH_2	Liquid Hydrogen
LHV	Lower Heating Value
LOHC	Liquid Organic Hydrogen Carrier
M	Million
m	meters
MCH	Methylcyclohexane
MeOH	Methanol
MGC	Medium Gas Carriers
MJ	Megajoule
n	Number of years
N	Number of compressor stages
n.a.	Not applicable
NG	Natural Gas
O&M	Operation and maintenance
OPC	Ortho-Para Conversion
OPEX	Operational Expenditure
OSBL	Outside battery limits
OSBL	Offsite
Pa	Pascal
PDBT	Perhydro dibenzyl toluene
PSA	Pressure Swing adsorption
Q_m	Molar flowrate
R	Universal gas constant
SEC	Specific Energy Consumption
Suc	Suction
T	Temperature
TCI	Total Capital Investment
TIC	Total installed costs
UC	Uninstalled costs
USD	US Dollars
X	Contingency
z	Compressibility factor

List of Figures

List of Tables

CONTENTS

1

INTRODUCTION

With the Paris Agreement in 2016, countries worldwide signed a treaty to limit global warming to below 2°C as compared to the pre-industrial levels. To mitigate climate change and achieve this target by 2050, global greenhouse gas emissions must be reduced significantly. Consequently, a great deal of effort is taking place in developing low-carbon solutions in the energy sector. The global capacity of renewable energy generation has increased from 2013 GW to 3068 GW over a span of six years after the Paris Agreement [45].

The intermittency of green electricity is one of the main drawbacks of renewable energy technologies, since most of them depend on the weather. As a result, energy storage technologies will be crucial in ensuring energy security as the world transitions away from fossil fuels. While numerous promising energy storage technologies, including batteries, pumped hydropower storage, compressed air energy storage, etc., are available, green hydrogen storage appears to be one of the leading solutions.

The reason hydrogen storage is considered very promising is because of its versatility and its potential to tackle critical challenges in the energy sector. Currently, hydrogen is the only option to decarbonize hard-to-abate sectors such as chemicals, long-haul transport, and the iron and steel sector [43]. Moreover, the chemical industry has years of experience in the production and handling of hydrogen. Furthermore, hydrogen can be transported as a compressed gas via pipelines, or in liquid form via ships. Alternatively, it can also be stored and transported in the form of other chemical compounds such as ammonia, methanol, etc. to capitalize on the use of existing infrastructure [41].

In the analysis carried out by IRENA, 12% of the final energy demand will be fulfilled by hydrogen by the year 2050 to achieve the goal of global warming reduction[46]. Renewable energy will be traded in the form of hydrogen between low-cost production sites and large energy demand centers. Although there will be several global centers for the import and export of hydrogen, it is anticipated that Germany, Japan, and the Netherlands would be the countries that import the most, while Australia will be the country that exports the

vast majority of hydrogen. [44].

The main issue related to the transportation of hydrogen is its lower volumetric energy density at ambient conditions. To tackle this problem, multiple promising options are being reviewed. In this report, the physical storage and transport of hydrogen as a compressed gas and liquified hydrogen will be explored. Additionally, circular hydrogen carriers such as green ammonia, green methanol, and Liquid Organic Hydrogen Carriers (LOHCs) will also be analyzed.

This aim of this report is to examine various hydrogen storage and transportation methods, and make an economical comparison. The analysis is done on a "Hydrogen to Hydrogen" basis in order to achieve a level playing field. Hydrogen obtained from an electrolyzer facility will be used as input for the analysis. Hydrogen is transported either in its physical form as compressed or liquefied hydrogen, or through chemical carriers. The hydrogen gas is converted into the chemical carriers in the hydrogenation plants. The carrier is then sent to the demand centers, where it will be converted back into hydrogen gas. The transportation pathways and hydrogen carriers examined in this report are depicted in Figure 1.1.

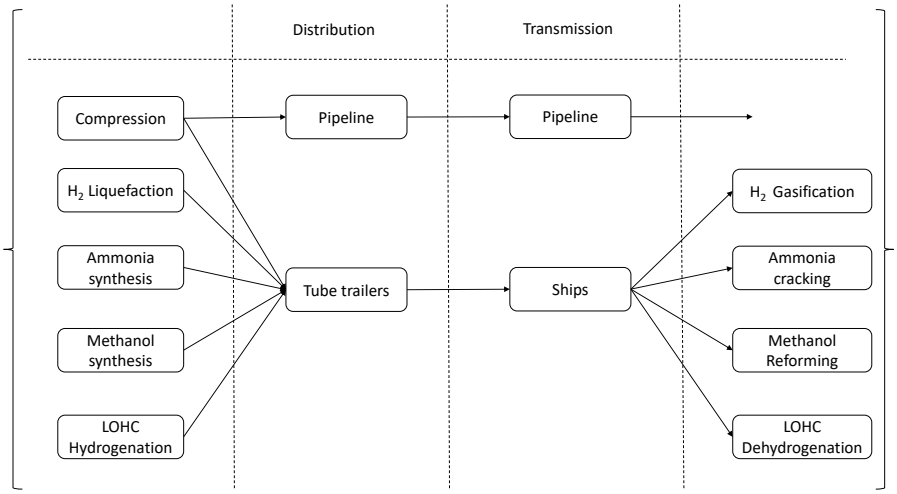

Figure 1.1: Hydrogen carriers and transportation pathways

The main research question this study addresses, is finding the hydrogen vector that has the lowest levelized cost of hydrogen (LCOH) for storage and transportation chain around different regions considering international supply chains. In order to achieve this, a preliminary literature review is carried out to investigate several hydrogen carrier methods. Afterward, using Unisim Design software, the hydrogenation and dehydrogenation processes for the selected carriers are simulated to examine critical factors including production

rate, raw material needs, and the specific energy consumption. Moreover, a cost analysis is performed for each technology to determine the individual overall capital investment cost. The data from the cost analysis and the Unisim Design simulations is then used to create a mathematical model in MATLAB, allowing the determination of the LCOH for each storage and transportation chain.

The literature review carried out for all the sections is documented in chapter 2. Modeling equations and simulations are documented in chapter 3 and chapter 4. Cost estimation for each technology is performed in chapter 5. Model results and sensitivity analysis are discussed in the chapter 6, along with the recommendations for future work. Finally, based on model results and sensitivity analysis, conclusions are drawn in the chapter 7.

2

LITERATURE REVIEW

In this chapter, a literature review is carried out for the most promising hydrogen storage technologies. Every carrier is reviewed for its physical and chemical characteristics, the hydrogenation and the dehydrogenation processes, as well as assumptions for transportation.

GASEOUS HYDROGEN

Compared to other fuels, hydrogen has one of the lowest volumetric energy densities at 0.011 MJ/L at standard temperature and pressure [75]. One of the most commonly used methods to increase the volumetric energy density of hydrogen is gas compression. Compressed gaseous hydrogen can be used to transport hydrogen over long distances via pipelines or trucks [74]. Despite being used widely, hydrogen compression is considered to be one of the most challenging and expensive units in the hydrogen supply chain [51].

Compression

Mechanical compressors are widely used in compression of gases, whereby mechanical energy is converted to compressed gas energy. Selection of compressor type depends on multiple factors such as the gas flow rate, final discharge pressure, pressure ratio between each stage, efficiency, operating temperature, gas composition, etc. A comprehensive review of different hydrogen compression technologies can be found in the review carried out by *Sdanghi et. al.*, [74].

Hydrogen is an extremely light gas with a molecular weight of 2.02 g/mol which is a major technical challenge for certain compressor types. In centrifugal compressors, kinetic energy of gas is converted to pressure using a high speed rotating impeller. Due to its low molecular weight relative to other gases, hydrogen requires the compressor to have extremely high tip speeds to accomplish the same pressure rise, since kinetic energy is a function of mass and velocity [18]. On the other hand, reciprocating compressors work on the principle of positive displacement and are therefore unaffected by the gas's molecular weight. Therefore, fewer number of stages are needed in reciprocating compressors

than in centrifugal compressors to attain the same pressure ratio. Hence, in the majority of applications, reciprocating compressors are currently the most effective choice for compressing hydrogen [4].

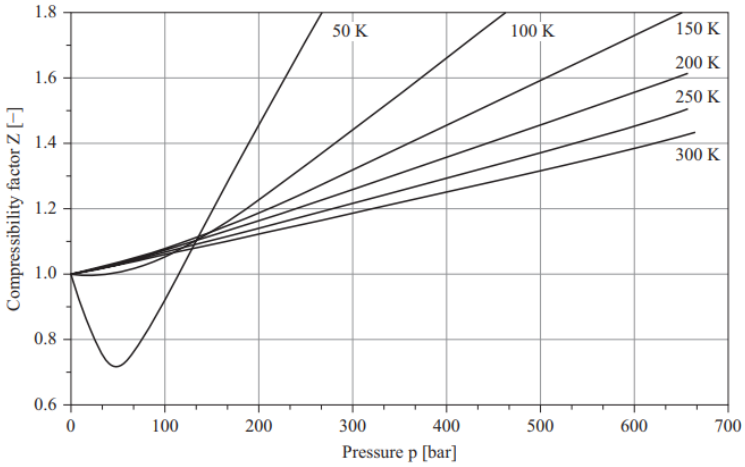

Figure 2.1: Compressibility factor of hydrogen

The thermodynamic behavior of most gases at different temperatures and pressures can be approximated by the ideal gas law. However, the behavior of hydrogen gas deviates significantly from the ideal gas law approximations [57]. Hydrogen gas occupies more space than the one predicted by the ideal gas law. Therefore, it is important to consider the compressibility factor (z) as a multiplier for the correction of the deviation while doing the power calculations for a hydrogen compressor. Compressibility factors for different temperature and pressure ranges are shown in Figure 2.1.

Hydrogen gas Pipelines

Hydrogen gas pipelines are an effective way to transport pure hydrogen from production sites to users. For transporting hydrogen via pipelines, two options can be considered.

- Building new pipelines for the transportation of hydrogen
- Modifying existing natural gas pipelines for transportation of hydrogen

Multiple studies have been carried out to assess the feasibility of using natural gas pipelines for hydrogen transport [59], [20]. These studies focus on technical issues such as the integrity and durability of pipelines, safety concerns, hydrogen embrittlement, and hydrogen leakage. The durability of pipelines may decrease when a high pressure and high concentration stream of hydrogen is introduced. The effect is largely dependent on the type of steel used in the construction of the pipeline, however, low-grade and more ductile steel pipelines are believed to have no hydrogen embrittlement at normal

operating conditions [59]. Research carried out by *Dodds et al.* to assess the feasibility of the UK gas system for hydrogen transport also concluded that high-strength steel is susceptible to hydrogen embrittlement and such pipelines are not suitable for hydrogen transport [28].

Hydrogen can be transported through existing pipelines with minor modifications to limit the hydrogen embrittlement. Countermeasures to avoid embrittlement noted in the literature include a chemical coating to protect the steel layer, pigging monitoring, management of operational pressure, and introduction of degradation inhibitors [5]. Moreover, peripheral equipment such as gas meters, control valves, valve fittings, gaskets, etc. needs to be adapted or replaced [36].

Higher upfront investment costs for the construction of new pipelines, make repurposing existing natural gas (NG) pipelines a more viable option. Research carried out by Siemens Energy concluded that the costs for converting existing gas pipelines for hydrogen transport are around 10-15% of the costs of construction of new pipelines [76]. The European Hydrogen backbone study concluded that the capital costs per kilometer of repurposed pipelines for hydrogen transport would be around 33% of newly built pipelines. Moreover, it also states that the CAPEX for new pipelines is 110 - 150% of natural gas pipelines with the same dimensions. In this study, total capital investment costs for new and repurposed pipelines are adapted from the report [5] and summarized in table 2.1.

Table 2.1: Total capital investments for different pipeline parameters taken from [5]

Pipeline	**Diameter (in)**	**Costs (M€/ km)**
New	<28	1.5
New	28 - 37	2.2
New	>37	2.8
Repurposed NG	<28	0.3
Repurposed NG	28 - 37	0.4
Repurposed NG	>37	0.5

Trucks and trailer

Gaseous hydrogen can be transported in pressurized cylinders or tubes. Multiple such tubes are bundled together in a tube trailer used to transport compressed hydrogen by road. The pressure inside these tubes may range between 180 and 350 bar. The transportation capacity of hydrogen via tube trailers is limited by the weight restrictions for road transport. Maximum allowable gross vehicle weight is fixed at 80,000 pounds in the U.S. and 40 tonnes in Europe [30].

Steel tube trailers are reported to carry around 380 kg of gaseous hydrogen, while newly developed composite material tube trailers can carry capacities of 560 to 900 kg of gaseous hydrogen [67]. Research is being carried out to increase the hydrogen payload of the trailers up to 1300 kg at elevated pressures. Moreover, 'Calvera Hydrogen', has recently developed the largest tube trailer for hydrogen transportation with a capacity of 1 ton at

Table 2.2: Assumptions and specifications for hydrogen trailer transportation taken from [66]

Parameter	Unit	Truck	Trailer
Payload	kg	n.a.	720
Speed	km/h	60	n.a.
Fuel consumption	L/100 km	30	n.a.
Capital Costs	€	160K	550K
O&M	%	12	2
Loading Time	h	n.a.	2

517 bar [32]. The hydrogen payload varies with the material of construction of the tank and the storage pressure. Specifications of tube trailers used in this study are summarized in the Table 2.2.

LIQUID HYDROGEN

The high gravimetric energy density of hydrogen with a lower heating value of 120 MJ/kg makes it a promising energy carrier [11]. However, hydrogen exhibits a poor volumetric energy density of approximately 8.5 MJ/L at ambient conditions, making its use difficult for long-distance transport and storage applications [35]. The volumetric energy density of hydrogen can be increased significantly by liquefaction.

In 1898, Sir James Dewar achieved hydrogen liquefaction for the first time by utilizing carbolic acid and liquid air for pre-cooling [27]. In 1902, Georges Claude invented the Claude cycle to liquefy hydrogen [53]. Barron explained that the 'Linde Hampson cycle' used for air liquefaction can be used to liquefy hydrogen with the implementation of liquid nitrogen precooling [13]. *Timmerhaus et al.* showed that 50% higher exergy can be achieved by the Claude system with a liquid nitrogen precooling cycle as compared to the Linde Hampson cycle.

Songwut et al. studied the development of large-scale hydrogen liquefaction processes, and the details of commercial plants worldwide can be found in the paper [53]. Linde commissioned the newest and largest hydrogen liquefaction plant in Germany in 2007. The plant operates on a nitrogen pre-cooled Claude system. The basic flow diagram of the Claude process is shown in Figure 2.2.

The main components of the liquefaction process are liquid nitrogen pre-cooling, cryogenic cooling, and Joule Thomson expansion valves. The standard liquefaction plant also includes absorbers to purify the hydrogen-rich stream received from the refinery. The gaseous hydrogen is liquified by the simultaneous conversion of normal hydrogen to para-hydrogen (OPC) using $FE(OH)_3$ catalyst followed by Joule Thompson expansion. The need and importance of OPC are explained in the following section.

The specific energy consumption of the industrially operating liquefaction plants is

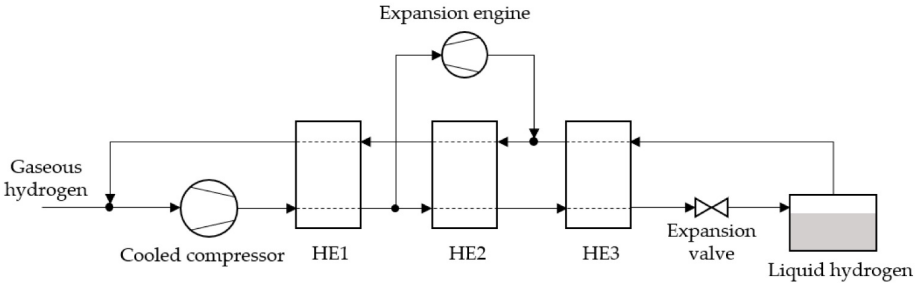

Figure 2.2: Basic flow diagram of Claude cycle

reported to be between 13 and 15 kWh/kg [53]. However, multiple conceptual design studies with different pre-cooling cycles have been carried out by different authors with SEC as low as 4 kWh/kg [54].

Ortho-Para Conversion

The hydrogen molecule has two spin isomers: ortho-hydrogen and para-hydrogen. At room temperature, the equilibrium composition of ortho-hydrogen and para-hydrogen is 75% and 25% respectively. However, with decreasing temperatures, ortho-hydrogen is gradually converted to para-hydrogen [77]. While the latent heat of the vaporization of hydrogen is around 445 J/g, the heat produced during OPC is higher at the value of approximately 527 J/g. This difference in the heat of conversion and vaporization leads to the boil-off of liquid hydrogen [70]. It is reported that 50% of liquid hydrogen will evaporate within 10 days if stored in the form of ortho-hydrogen. Hence, to avoid boil-off, ortho-hydrogen is converted to para-hydrogen in the liquefaction process itself. More than 95% conversion to para-hydrogen is achieved in such OPC reactors that subsequently minimize the hydrogen boil-off.

Evaporation

For the final use of hydrogen, it needs to be regasified at the end of the storage and transportation chain. A vaporizer unit is typically used in the regasification process, where liquid hydrogen can be easily converted to gaseous hydrogen.

Liquid Hydrogen Transport

In December 2019, Kawasaki Heavy Industries Ltd. introduced the world's first liquid hydrogen carrier ship "Susio Frontier" to transport hydrogen over long distances [50]. In February 2022, the ship successfully transported liquid hydrogen produced in Australia to the port of Kobe, Japan [39]. Similar to compressed gas, liquid hydrogen can also be transported via trucks on land. Specifications and assumptions for liquid hydrogen transport vehicles are shown in Table 2.3.

Table 2.3: Assumptions and specifications for liquid hydrogen transportation [66]

Parameter	Unit	Truck	Trailer	Ship
Payload	kg	n.a.	4500	12658
Speed	km/h	60	n.a.	32
Fuel cons.	L/100 km	30	n.a.	9.26
Capital Costs	M€	0.16	0.86	412
O&M	%	12	2	2
Loading Time	h	n.a.	3	2

GREEN AMMONIA

With an energy consumption of 8.6 EJ in 2020, global ammonia production accounted for around 2% of total final energy consumption. This energy consumption also corresponds to 450 Mt of CO_2 emissions [42]. These higher emission numbers are due to the use of fossil fuels in reformers to produce hydrogen. However, low-carbon production technologies such as electrolysis, methane pyrolysis, and traditional plants with carbon capture technology are emerging as promising options.

Liquid ammonia can be stored at -33 °C at atmospheric pressure, or it can be stored under high pressure at ambient temperature. While 70 to 80% of produced ammonia is used for the production of fertilizers, it is also used as a refrigerant, manufacturing of explosives, dyes, pesticides, etc [24]. In the energy transition, ammonia is expected to play a role as a hydrogen carrier, transportation fuel, and a thermal fluid to store thermal energy [79]. A global market size of 63 billion USD in 2022 [81] , and existing storage and transportation infrastructure, make liquid ammonia an attractive option for the energy transition.

Developed by Fitz Haber and industrialized by Carl Bosch in 1908, the Haber - Bosch ammonia synthesis method is widely used for ammonia production to date. In this process, gaseous hydrogen and nitrogen react over an iron catalyst at a temperature range of 400 to 500 °C and a pressure range of 100 to 250 bar. Since its introduction in the early 1900s, the ammonia synthesis process has changed very little. However, the process has been optimized significantly from about 100 GJ/Ton NH_3 energy requirements in the early 1900s to about 26 GJ/ton NH_3 today [71]. The exothermic ammonia synthesis reaction is as follows:

$$N_2 + 3\,H_2 \longrightarrow 2\,NH_3 + 46.1\,kJ/mol$$

The main production steps involved in the Haber Bosch synthesis are hydrogen and nitrogen production, syn gas purification, syn gas compression, and ammonia synthesis. The key difference between the traditional Haber Bosch process and up-and-coming sustainable processes is mainly the method of hydrogen production. A basic flow diagram for the green ammonia concept is depicted in the Figure 2.3.
The energy requirement for traditional Haber Bosch plants is reported to be between 8 - 12 MWh/ton NH_3 depending on the reformer feedstock. The energy consumption of 7.8 MWh/ton is the least for natural gas, followed by coal and oil with the energy

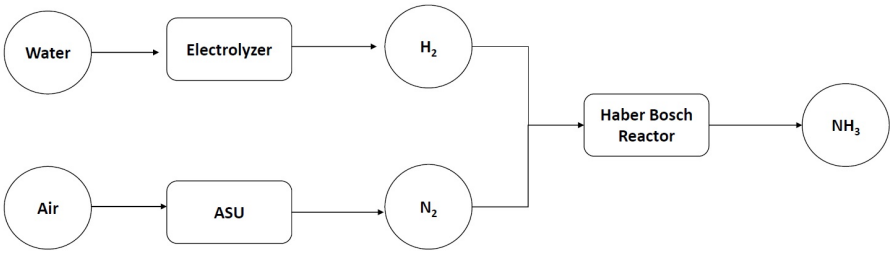

Figure 2.3: Green Ammonia concept

consumption of 10.6 and 11.7 MWh/ ton NH_3 respectively [72]. The energy consumption range of green ammonia plants is expected to be higher than the natural gas feedstock, with the requirement of 10 - 12 MWh/ ton NH_3 [17].

Liquid Ammonia Transportation

Global transportation and storage infrastructure for liquid ammonia is already in place, which gives liquid ammonia a slight edge as compared to other hydrogen vectors. By the year 2025, around 20 million metric tons of ammonia are expected to be traded worldwide [78]. Ammonia can be transported inland via pipelines, truck trailers, and trains, while transported via carrier vessel ships across the sea.

In the USA, NuStar Energy has established an ammonia pipeline network of 2000 miles, that transports 1.5 million tonnes of ammonia annually [6]. Around 2.5 million tonnes of ammonia used to be transported from the Volga region of Russia to the Black Sea port of Pivdennyi in Ukraine, which is currently shut down due to the ongoing war situation [25].

Similar to hydrogen gas pipelines, the costs of ammonia pipelines depend on the distance, ammonia throughput, temperature, and elevation difference. A very limited amount of data is available for the aforementioned factors, which makes it difficult to make a cost estimation for pipeline transport. Thus, ammonia transport via pipelines is excluded from this study. Similarly, transport via trains is subject to the availability of the existing railway line network, and hence, not considered.

For long distances over the sea, ammonia transportation is typically carried out via gas carrier vessels. Depending upon the volume, the vessels are categorized as "Medium Gas Carriers" (MGCs) and "Large Gas Carriers" (LGCs). The corresponding volume ranges for the carriers are 20,000 to 45,000 m3 and 45,000 to 65,000 m^3 respectively [64]. Typical characteristics of the vessels used in the calculations are shown in Table 2.4.

Table 2.4: Assumptions and specifications for liquid ammonia transportation [66], [62]

Parameter	Unit	Truck	Trailer	Ships		
				Unit	MGC	LGC
Payload	kg	n.a.	14500	ton	23000	39000
Speed	km/h	60	n.a.	km/h	28	30
Fuel consumption	L/100 km	30	n.a.	ton/day	37	37
Capital Costs	€	160K	860K	$ / day	28000	38500
O&M	%	12	2	%	2	2
Loading Time	h	n.a.	2	h	48	48

Liquid Ammonia cracking

Conversion of ammonia back to hydrogen is carried out by ammonia cracking. While ammonia cracking is not yet operational at a commercial scale, experimental studies are reported in the literature for ammonia cracking. The decomposition reaction of ammonia to hydrogen is as follows :

$$2\,NH_3 \longrightarrow N_2 + 3\,H_2 - 92\,kJ/mol$$

Makhloufi et al. designed an ammonia cracking plant to produce 200 MTPD of pure hydrogen with a thermal efficiency of 68.5% and a specific energy consumption of 12.65 MJ/nm^3 [56].

Membrane reactors are a promising technology for ammonia cracking as well as methanol reforming, with very high conversion rates as compared to traditional fixed bed reactors [52], [19]. The working principle of the membrane reactors can be explained via the Figure 2.4.

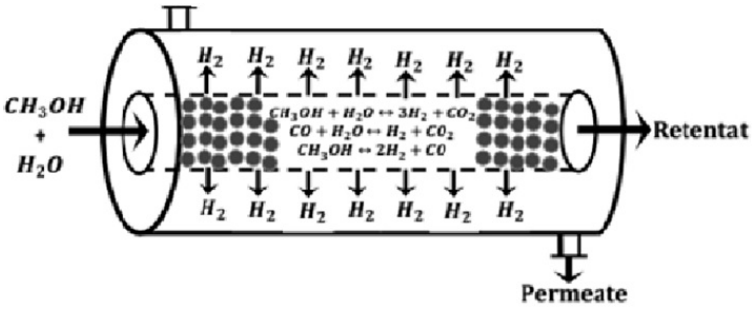

Figure 2.4: Membrane reactor working principle

The membrane reactor consists of a reactor and a hydrogen separator in a single unit, thus eliminating the need for a separate hydrogen purification unit. The product hydrogen

is continuously removed with the help of a membrane along the length of the reactor. Continuous removal of hydrogen results in a shift of equilibrium towards the right, leading to higher reactant conversion and hydrogen yield [19]. However, in the UniSim Design R471 software, it is not possible to simulate a membrane reactor. Hence, a traditional packed bed rector will be used to simulate ammonia cracking in this report.

Green Methanol

Methanol is gaining a lot of attention as a cleaner alternative to traditional fossil fuels. Methanol has a gravimetric energy density of 20.1 MJ/kg and a volumetric energy density of 4.33 kWh/L [16]. It is liquid at room temperature, less toxic, and hence easier and safer to transport as compared to other hydrogen carriers such as Ammonia [22].

For the production of green methanol, hydrogen is obtained from a green path such as electrolysis and biomass gasification, etc. CO_2 can either be captured from traditional plants, biomass, or directly from the air. Capturing CO_2 from traditional plants will help in reducing CO_2 emissions of hard-to-abate sectors like steel production.

Green methanol technology has been successfully applied in small-scale demonstration plants in Germany, Denmark, and Iceland [23]. Recently, the first large-scale commercial green methanol plant has been commissioned by Carbon Recycling International (CRI) in China. This facility in Anyang, Henan Province, has successfully started production and is expected to produce 100,000 metric tonnes of green methanol annually, simultaneously capturing 160,000 tonnes of CO_2 per year [14], [73].

The main disadvantage associated with green methanol technology is the release of CO_2 if methanol is utilized or decomposed directly. Moreover, CO_2 separation techniques such as absorption using amine solution are energy-intensive processes [12].

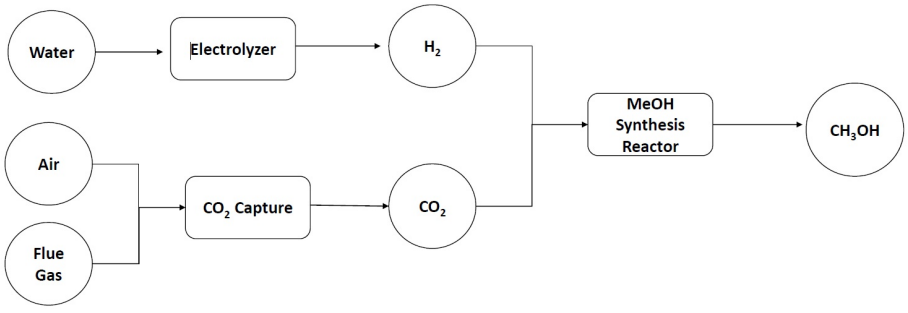

Figure 2.5: Green Methanol concept

Methanol is synthesized via the hydrogenation of CO_2 in presence of a catalyst. The reaction temperature and pressure are between 210 - 270 °C and 50 to 100 bar respectively [23][38]. The molar ratio of H_2/CO_2 is 3. The main methanol synthesis reaction is as follows:

$$CO_2 + 3\,H_2 \longrightarrow CH_3OH + H_2O + 49\,kJ/mol$$

The H_2 and CO_2 mixture is preheated before entering the synthesis reactor. Unreacted gases are separated from the reactor outlet stream and recirculated back to the reactor. The liquid product consists of methanol and water, which is passed through a series of distillation columns to obtain pure methanol. In conventional methanol plants, 2-4 distillation columns are used to obtain pure methanol. However, in green methanol plants, fewer impurities are present, subsequently reducing the number of required distillation columns [23].

METHANOL DECOMPOSITION

Hydrogen can be produced from methanol via different conversion pathways such as via steam reforming, partial oxidation, auto thermal reforming, and methanol decomposition. *Garcia et al.* conducted a comprehensive review of these technologies and compared different performance parameters [33]. While each of the technologies has its own advantages and disadvantages, methanol steam reforming is the most established process with high methanol conversion, higher yield, and low CO generation. Methanol steam reforming will be used as the base technology for hydrogen production in this report.

Multiple studies have been carried out for methanol steam reforming using a conventional packed bed reactor. The challenges associated with the reforming in PBR are high operating temperature and the need for additional H_2 purification using pressure swing adsorption (PSA) leading to higher capital costs [52], [19]. To overcome these barriers, membrane reactors for methanol reforming are gaining a lot of attention.

A membrane reactor consists of a reformer and H_2 separator membranes in a single unit, eliminating the need for PSA and consequently reducing capital costs [19]. During the reaction, produced H_2 is continuously separated through membranes driven by differences in partial pressures. Hence, equilibrium is shifted towards the right according to Le Chatelier's principle, leading to improved methanol conversion [52].

Methanol steam reforming reaction is as follows:

$$CH_3OH + H_2O \longrightarrow CO_2 + 3\,H_2 + 131\,kJ/mol$$

The reforming temperature ranges from 473 to 537 K, and the pressure is between 1 and 3 bar.

LOHC

Liquid Organic Hydrogen carriers are the organic compounds that exist in liquid phase at ambient conditions, or solids with lower melting point, and can absorb and release hydrogen through chemical reaction [82]. Most promising LOHCs are dibenzyl toluene - perhydro dibenzyltoluene, toluene - methylcyclohexane, and N-ethylcarbazole - perhydro - N- ethylcarbazole among others. Some authors also consider methanol as a LOHC. However, in the methanol system, after dehydrogenation CO_2 gas is released. Hydrogen

carriers such methanol, formic acid are referred to as "circular carriers", since gas molecules used for synthesis of hydrogen carrier are captured from the atmosphere and released back after dehydrogenation, completing a circle [3].

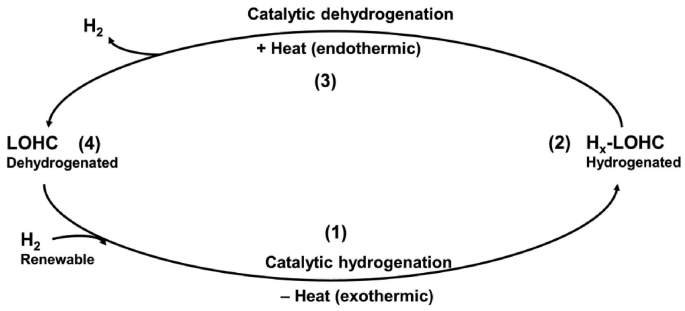

Figure 2.6: LOHC hydrogenation and dehydrogenation [65]

A schematic representation of LOHC chain is depicted in Figure 2.6. Hydrogen lean LOHC is "loaded" with hydrogen at production site. LOHC hydrogenation is an exothermic reaction. The charged liquid LOHC is then transported to the end user via different transportation routes. At the user end, hydrogen is released from the liquid carrier in presence of a catalyst. LOHC dehydrogenation reaction is an endothermic reaction and requires external heat supply. The initial structure of the LOHC compound is restored after the loaded hydrogen is released. After dehydrogenation, the "unloaded" LOHC is then transported back to the production site [2].

Amongst different LOHC options, extensive studies are carried out on the DBT system. Moreover, "Hydrogeneous technologies" have successfully demonstrated the use of DBT system for hydrogen supply. Similarly, toluene and MCH are already widely used in the chemical industry. Hence, Dibenzyltoluene system and toluene- MCH system will be considered in this report, which seem to be the most promising LOHC systems.

Due to its physicochemical characteristics, such as its low volatility and good thermal stability, dibenzyltoluene is being used as a heat transfer oil [49][10]. *Ali et al.* investigated the hydrogenation of DBT with different catalysts at 0.80 MPa [9]. The results indicated 170 °C as the optimum temperature for the reaction over Raney- Ni catalyst. *Jorschick et al.* proposed a mixture of H12-BT and PDBT to address challenges occurring due to high viscosity of PDBT. The experiment concluded that the mixture enhances hydrogen release productivity by 12-16% as compared to pure PDBT [49]. A typical DBT LOHC system is shown in Figure 2.7.

MCH is a versatile organic solvent and is extensively used in the chemical industry [83]. Hydrogenation of toluene is an exothermic reaction which is carried out at 180-200

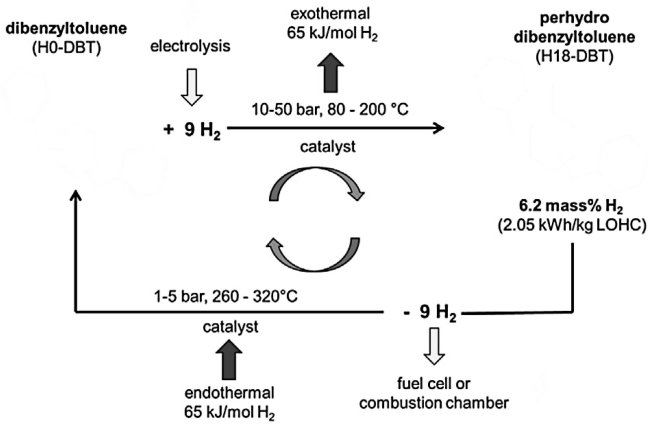

Figure 2.7: LOHC - DBT and PDBT system [65]

°C under 5 - 7 MPa pressure [83]. Dehydrogenation of MCH, on the other hand, is an endothermic reaction favored at low pressures and high temperatures. At 350 °C and 2 bar, about 99.5% conversion can be achieved [68]. A typical toluene- MCH LOHC system is shown in the Figure 2.8.

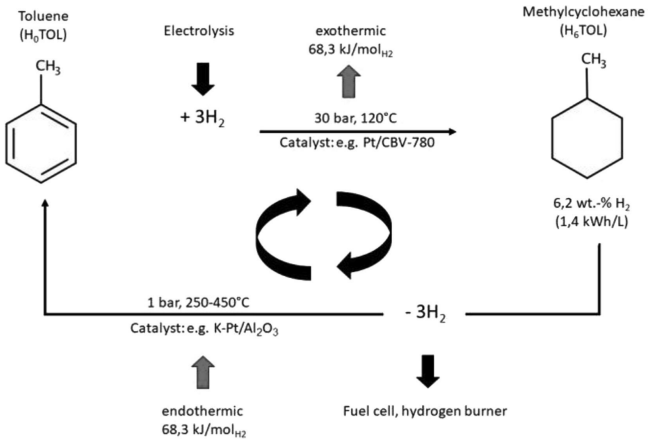

Figure 2.8: LOHC - Toluene and MCH system [65]

Methanol and LOHC transportation

As previously discussed, it is debatable whether methanol can be considered a LOHC. However, the study uses the same set of assumptions for both methanol and other LOHCs when assessing their transportation via trailers and ships. The assumptions and specifications used for methanol and LOHC transportation are summarized in the table 2.5:

Table 2.5: Assumptions and specifications for methanol and LOHC transportation [66]

Parameter	Unit	Truck	Trailer	Ship
Payload	Ton	n.a.	4.50	1250
Speed	km/hr	60	n.a.	32
Fuel consumption	L/100 km	30	n.a.	9.58
Capital Costs	€	160K	860K	$412x10^6$
O&M	%	12	2	2
Loading Time	h	n.a.	3	48

Energy density and hydrogen content summary

The summary of storage conditions, energy density, and hydrogen content of the considered hydrogen vectors is tabulated in Table 2.6.

Table 2.6: Summary of energy density and hydrogen content for different hydrogen vectors [26], [47], [65]

Vector	Storage Temperature (°C)	Storage Pressure (MPa)	Volumetric energy density (MJ/L)	Gravimetric Hydrogen content (wt%)	Volumetric Hydrogen content (kg H_2/m^3)
Ambient H_2	25	0.10	0.01	100	0.09
Compressed H_2	25	20.00	2.16	100	18
Liquiefied H_2	-253	0.10	8.49	100	70.8
Ammonia	-33	0.10	12.82	17.8	121.4
Methanol	25	0.10	15.80	12.5	99.4
PDBT	25	0.10	6.84	6.2	56.6
Toluene	25	0.10	5.76	6.2	47.40

International hydrogen trading routes

To achieve the goal of global warming reduction by the year 2050, 12% of the global final energy demand will be fulfilled by hydrogen [46]. It is expected that the hydrogen will be traded as a commodity across different countries across the globe. Depending on the local hydrogen demand, production volumes, and cost of production, there will be hydrogen import and export hubs [44]. The hydrogen export and import indices for regions around the world in the year 2050 are shown in Figure 2.9.

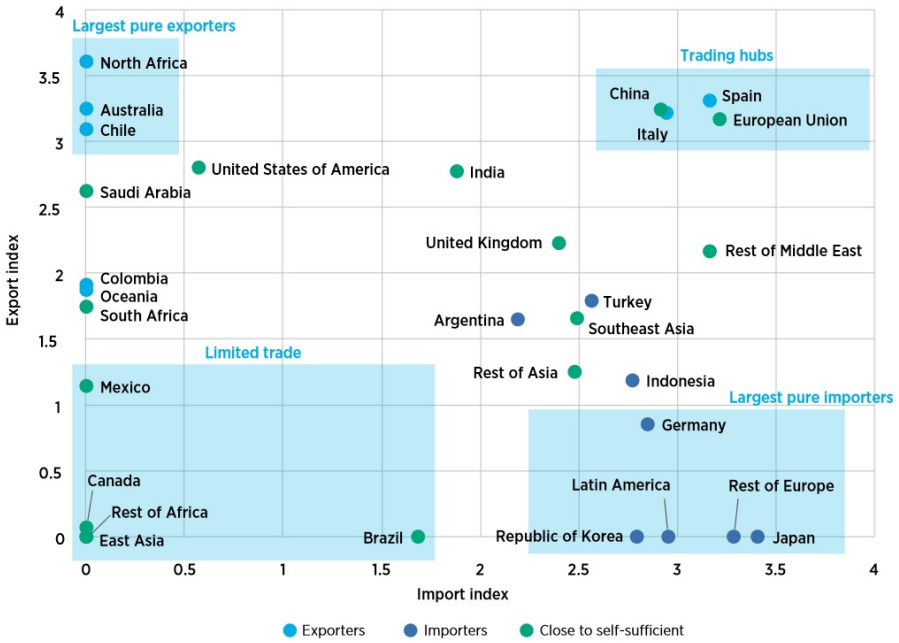

Figure 2.9: Hydrogen trading indices for regions in the year 2050 [44]

Based on the trade overview obtained from this, the countries for the export and import of hydrogen are selected for this study. The distance between the hydrogen production facility and the port, which is referred to as 'distribution' distance, and the overseas port to port distance between the trading countries, referred to as 'transmission' distance in this study is also summarized in Table 2.7:

Table 2.7: Hydrogen trading routes adapted in this study

Route	Hydrogen Exporter	Hydrogen Importer	Distribution distance (km)	Transmission distance (km)
1	Australia	Japan	150	9000
2	Chile	USA	36	13460
3	Egypt	The Netherlands	12	7365
4	Saudi Arabia	Germany	100	9850

3

MODEL DEVELOPMENT

A mathematical model is built in MATLAB to calculate the LCOH of each hydrogen vector and transport route. The overall hydrogen storage and transportation supply chain consists of different steps such as conversion of hydrogen to a hydrogen vector, land transport of the vector to the port and overseas transport via ships, and again conversion back to gaseous hydrogen. LCOH of each steps of the supply chain is calculated individually to finally get the overall LCOH of the chain. To calculate LCOH, the three major cost elements required are CAPEX, fixed OPEX, and variable OPEX. Each of these elements are explained in the upcoming sections. Detailed model assumptions are documented in Appendix A.

HYDROGENATION AND DEHYDROGENATION PLANTS

Annual CAPEX

To determine the annualized CAPEX of a production plant, the first step is to calculate the fixed capital investment for the plant. Calculation of fixed capital investment costs will be explained in detail in chapter 5. The calculated fixed capital investment costs are converted to annualized CAPEX using a Capital Recovery Factor (CRF). The CRF for the discount rate "i" and number of years "n" is given as:

$$CRF = \frac{(i(1+i)^n)}{((1+i)^n - 1)} \tag{3.1}$$

The annualized CAPEX in €/year is given by:

$$CAPEX\ (€/year) = (CRF) * Total\ Capital\ Investment \tag{3.2}$$

Annual OPEX

The annual OPEX is primarily divided into two components: fixed OPEX and variable OPEX. Fixed OPEX are the costs that are incurred irrespective of whether the plant is running or not. These costs typically include the maintenance costs, plant overhead costs,

insurance costs, etc. In this report, the fixed OPEX are taken as a fixed % of the fixed capital investment costs.

Variable OPEX are the costs that vary depending upon the production rate of the plant. These costs typically include the costs of raw materials, utilities, etc. In this report, the costs associated with electricity consumption are considered as the variable operating costs. Moreover, the costs of raw materials and chemicals are also considered wherever applicable. The costs of utilities such as steam, instrument air, cooling water, etc. are neglected in the calculations for simplification. The quantity of energy requirement and raw materials is obtained from the Unisim simulations of respective pathway. Annual OPEX is given as:

$$Annual\ OPEX\ (€/year) = OPEX_{fixed} + OPEX_{variable} \tag{3.3}$$

Levelized Cost of Hydrogen (LCOH)
Once all of the above cost components are obtained, the LCOH of the pathway is calculated as:

$$LCOH_{production}\ (€/kg H_2) = \frac{Annual\ CAPEX + Annual\ OPEX}{Annual\ Hydrogen\ Produced\ (kg)} \tag{3.4}$$

TRANSPORT ON ROAD

Road transport of all the carriers is done via tube trailers that are mounted on top of the trucks except for compressed hydrogen, where pipeline transport is also considered. Considering the speed of the truck, and the distribution distance, time required for one tube trailer is calculated for the entire journey. It should be noted that the calculation is done for a two-way journey, that is, transport of the hydrogen carrier to the port and return journey of the empty truck back to the production site. Moreover, time required for loading the trailers is also considered in this calculation. Additionally, 10% of contingency is also considered accounting for road traffic, reroutes, etc.

$$Trailer\ journey\ time\ (h) = (\frac{(2 * Distance)}{Truck\ speed} + Loading\ time) * Contingency \tag{3.5}$$

Considering the truck journey time and payload of the truck trailers, the quantity of carrier transported daily via one trailer can be calculated. Furthermore, it is used to determine the number of trailers required per day to transport all the carrier produced daily.

$$N_{trailers} = \frac{Daily\ carrier\ production}{Daily\ quantity\ transported\ via\ one\ trailer} \tag{3.6}$$

Assuming that the truck trailers are operating round the clock, the annual number of trips for each trailer can be calculated from the journey time for one trip. Moreover, annual fuel consumption from all the trailers can be calculated as:

$$Annual\ fuel\ consumption\ (l/year) = 2 * Distance * Fuel_{CR} * Annual\ journeys * N_{trailers} \tag{3.7}$$

Here, $Fuel_{CR}$ is the fuel consumption rate of the truck in L/km. Annual fuel costs are considered as the variable OPEX in the LCOH calculation for road transport. Annual CAPEX and fixed OPEX are calculated by the same methodology as stated in the previous section. Finally, the LCOH for road transport is given as:

$$LCOH_{distribution}\,(€/kgH_2) = \frac{Annual\,CAPEX + Annual\,OPEX}{Annual\,Hydrogen\,Delivered\,(kg)} \tag{3.8}$$

Transport overseas

All other carriers are transported overseas via ships, except for gaseous hydrogen. The payload, speed, fuel consumption of ships differ from carrier to carrier, and are mentioned in the respective literature section in chapter 2. One of the key difference that should be noted is that due to existing transportation infrastructure of ammonia, it is possible to charter the ammonia ships, rather than purchasing. However, for other carriers, fixed capital costs need to be considered for purchasing the ships.

Similar to the calculations for truck trailers, journey time for one ship is calculated by considering the ship speed, loading time, and a contingency. The time is calculated for the two-way journey of the ship. For simplicity, the speed and fuel consumption are assumed to be constant for loaded as well as the unloaded ship.

$$Ship\,journey\,time\,(h) = (\frac{(2 * Distance)}{Ship\,speed} + Loading\,time) * Contingency \tag{3.9}$$

To determine the number of ship required annually, first the annual number of trips is calculated based on the carrier's total annual production and the capacity of a single ship. Additionally, the maximum number of trips a single ship can make is also calculated, taking into account the duration of a single journey. If the total annual trips required are less than the maximum possible trips, a single ship can handle all the carrier's transportation needs for the year. However, if this is not the case, the following equation is used to calculate the number of ships needed. The answer is rounded off to the next higher integer.

$$No.\,of\,ships\,required = \frac{Total\,annual\,trips}{Maximum\,possible\,trips\,for\,one\,ship} \tag{3.10}$$

The $LCOH_{transmission}$ for shipping is determined from the Equation 3.8.

H_2 compression

For H_2 compression, fairly accurate numerical models are already available in the literature, and it was decided to adapt a similar numerical model. To achieve higher pressures, compression is carried out in multiple stages with compression ratios greater than 2. Thermodynamic power calculations for multistage hydrogen compressors are done using

the isentropic model provided by *Khan et al.* [51]. The model incorporates several assumptions, such as the pressure ratio and the work done at each stage being equal. Moreover, after each stage, the temperature of the gas is cooled to the suction temperature of the first stage. Finally, the model ignores the pressure drop and heat losses between the stages.
The number of compressor stages (N) can be calculated by the equation:

$$N = \frac{log(\frac{P_{dis}}{P_{suc}})}{log(x)} \tag{3.11}$$

The isentropic power of the compressor is calculated as:

$$P_{isen}\,(kW) = N * \frac{k}{k-1} * \frac{z}{n_{isen}} * T_{suc} * Q_m * R * [(\frac{P_{dis}}{P_{suc}})^{(\frac{k-1}{N*k})} - 1] \tag{3.12}$$

Where, k is H_2 polytropic coefficient (1.41), z is the compressibility factor, n_{isen} is the isentropic efficiency of the compressor assumed to be 88%, R is the universal gas constant 8.314 J/mol.K, T_{suc} is the suction temperature in kelvin, Q_m is the molar flow rate of hydrogen in mol/s, P_{dis} and P_{suc} are the discharge and suction pressure of the compressor in bar respectively. Finally, rating of the compressor (motor) is calculated as:

$$P_{compressor}\,(kW) = \frac{P_{isen}}{n_{motor}} \tag{3.13}$$

Annual electricity costs for the compressor are determined by the following equation, where LCOE is the Levelized Cost of Electricity, and 8760 is the annual number of hours.

$$Electricity\,Costs\,(€/year) = P_{compressor} * 8760 * LCOE \tag{3.14}$$

The uninstalled costs of the compressor are calculated by the relation adapted from HDSAM given by [60]:

$$UC_{compressor}\,(€) = 21,224 * (P_{compressor})^{0.6089} \tag{3.15}$$

The obtained costs in USD are normalized to €2022 using CEPCI and currency exchange rate [58], [31]. Total installed costs are calculated using the following relation:

$$TIC_{compressor}\,(€) = UC_{compressor} * Installation\,Factor \tag{3.16}$$

An installation factor of 1.3 is assumed for the compressor. Additionally, 40% indirect costs are also considered to finally obtain the total capital investment of the compressors.

$$TCI_{compressor}\,(€) = TIC_{compressor} + Indirect\,Costs \tag{3.17}$$

From total capital investment, annual CAPEX, OPEX, and LCOH for the compressor are calculated from the Equation 3.2, Equation 3.3, and Equation 3.4 which are explained previously.

It is assumed that after every 250 km, there is a booster compressor station. Hence, based on the total distance, the number of booster compressor stations is determined. Calculations for booster compressors are performed similarly to the main compressor from Equation 3.11 to Equation 3.17.

Liquid hydrogen evaporator

At the end of the liquid supply chain, liquid hydrogen is regasified by using an evaporator. A numerical model is adapted for the evaporator from HDSAM, similar to compressed hydrogen [60].

$$UC_{evaporator}\ (€) = 128.32 * Q + 94,766 \tag{3.18}$$

Here, $UC_{evaporator}$ is the uninstalled cost for the evaporator normalized to €2022, and Q is the hydrogen flow rate in kg/hr.

$$TIC_{evaporator}\ (€) = UC_{evaporator} * Installation\ Factor \tag{3.19}$$

The installation factor for the evaporator is assumed to be 1.3. The total capital investment, annual CAPEX, OPEX, and LCOH are calculated using the same relationships used for the compressor.

Intermediate storage considerations

To avoid any disruptions in production, storage tanks are assumed to be in place to provide a buffer. It is assumed that for each carrier, there is one storage tank on either side of the supply chain: one storage tank at the port of the exporting country, and one storage tank in the country of destination. For LOHCs, there are two storage tanks on either end. For instance, if the toluene-MCH system is considered, there are storage tanks for both toluene and MCH on both ends of the supply chain. Finally, it is assumed that the tanks have a capacity to store for 60 days. The cost assumptions for storage technologies are summarized in Table 3.1:

Table 3.1: Cost assumptions for storage tanks

Carrier	Storage cost	Unit	Reference
LH_2	31	€/kg LH_2	[66]
Ammonia	0.95	€/kg NH_3	[62]
Methanol	237	€/m^3 MeOH	[66]
LOHCs	237	€/m^3 LOHC	[66]

CO_2 storage and transportation

During the production of hydrogen via methanol reforming, CO_2 is released as a by-product. This CO_2 cannot be vented to the atmosphere due to environmental considerations. Hence, it must be liquified and transported back to the country where methanol production takes place to be utilized in the methanol synthesis process. The team at 'European Technology Platform for Zero Emission Fossil Fuel Power Plants' analyzed the costs of CO_2 liquefaction, storage and transportation for shipping distances of 180, 500, 750 and 1500 km [29]. The results of this study are extrapolated to define the following relation between the shipping cost (€/ton CO_2) and shipping distance (km):

$$CO_{2\,shipping}\ (€/tonCO_2) = 0.0038 * (Distance) + 10.356 \tag{3.20}$$

It should be noted that the CO_2 shipping cost obtained here consist of cost of liquefaction, storage, and overseas transportation, which are then added to cost of methanol supply chain.

LCOH OF THE ENTIRE SUPPLY CHAIN

Once the LCOH of each step of the supply chain is calculated individually, these values are combined to obtain the overall LCOH of the entire supply chain.

$$\begin{aligned} LCOH\,(€/kgH_2) = & LCOH_{production} + LCOH_{distribution} + LCOH_{trasnmission} \\ & + LCOH_{reconversion} + LCOH_{storage} \end{aligned} \tag{3.21}$$

CARBON EMISSIONS

In this analysis, scope 1 CO_2 emissions will be considered. These emissions come from equipment that are within direct ownership of the organization. Emissions from the on-site combustion of fuels for operations and heating systems, and company-owned vehicles, are the scope 1 emissions that are taken into consideration. Total annual CO_2 emissions are calculated as:

$$Annual\ CO_2\ emissions\,(tons) = Annual\ fuel\ consumption * EF_{fuel} \tag{3.22}$$

Here, for industrial heating, fired heaters with natural gas as fuel are considered. Moreover, depending upon the mode of transportation, diesel and heavy fuel oil are considered as a fuel. EF represents the emission factor of the associated fuel. The unit of annual fuel consumption may be m^3 or ton, and the corresponding unit for emission factor is ton CO_2/ m^3 fuel, or ton CO_2/ ton fuel.

$$Annual\ CO_2\ emission\ cost\,(€/year) = Annual\ CO_2\ emissions * Carbon\ credit\ cost \tag{3.23}$$

From Equation 3.23, annual costs for CO_2 emissions are calculated. A carbon credit cost of 90€/ton CO_2 is assumed for the analysis.

4

PROCESS SIMULATIONS

Process simulations of all the proposed pathways are carried out using the UniSim Design R471 software. UniSim Design R471 is a software developed by Honeywell that is widely used for steady-state and dynamic process simulations and modeling [61]. All the simulations will be explored one by one in the following sections. Detailed stream properties and compositions for all simulations can be found in Appendix C.

GASEOUS HYDROGEN - COMPRESSION

To transport gaseous hydrogen via pipelines, it is compressed up to 180 bar in a compressor. A multi-stage reciprocating compressor is used to simulate the process. The process flow diagram for hydrogen compression is shown in Figure 4.1.

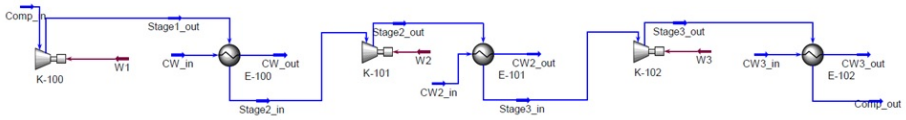

Figure 4.1: Hydrogen compression process flow diagram

The process conditions of the hydrogen gas at the inlet of the compressor are 30 bar and 35 °C. After each compression stage, the gas is again cooled down to 35 °C with the help of intercoolers. Finally, the outlet gas is also cooled to 35 °C via an aftercooler before it can be transported via gas pipelines. The assumptions made for the simulations are listed below :

- The adiabatic efficiency of the compressor is 80%.
- There is no pressure drop in the intercoolers.

- The inlet and outlet temperatures of the cooling water stream are 30 °C and 45 °C respectively.
- Maximum allowable temperature for any compressor stage outlet is limited to 135 °C.
- Compression ratio for all the stages is equal.
- Pure hydrogen gas is compressed, i.e. there is no moisture content in the feed.

The simulation results are summarized in the following table:

Table 4.1: Hydrogen compression simulation results

Description	Value	Unit
No of stages	3	
Compression ratio	1.82	
T_out	35	°C
P_out	180	bar
Power rating	1603	kW

HYDROGEN LIQUEFACTION

The liquefaction of hydrogen is carried out in a series of multi-stream cryogenic heat exchangers. Hydrogen is liquefied at the temperature of -253 °C at atmospheric pressure. Such low temperatures can be achieved using the helium Brayton cycle. The helium gas in compressed to 6 bar using a 3 stage reciprocating compressor with intercoolers. The compressed helium gas, after passing through the cryogenic heat exchangers, is expanded to atmospheric pressure in an expansion turbine. The expansion of the helium gas leads to a drop in the temperature up to -255 °C. The low temperature stream is used to cool the hydrogen stream to its liquefaction temperature.

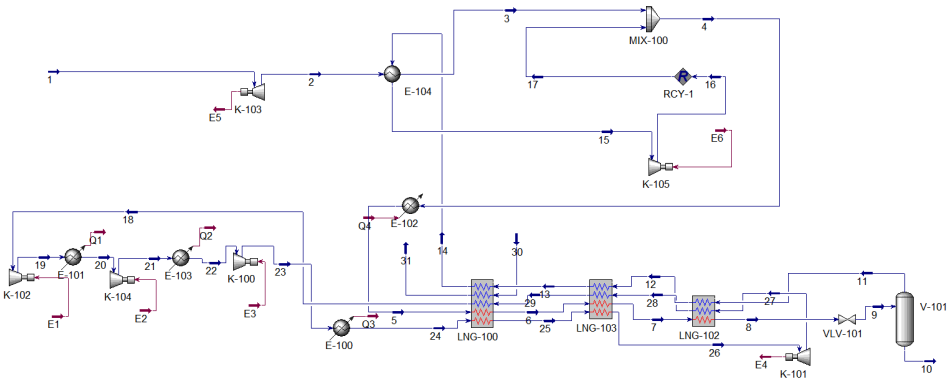

Figure 4.2: Process flow diagram of simulated hydrogen liquefaction process

The helium gas stream after passing through the cryogenic heat exchangers is recirculated back to the compressors. Additional cooling duty for the hydrogen gas and the compressed helium gas in the first cryogenic heat exchanger is provided by liquid nitrogen. After recycling the hydrogen vapors back into the system, 100% of the gaseous hydrogen is liquefied, with an SEC of 8.93 kWh/ kg LH_2.

Ammonia Synthesis

Ammonia synthesis is carried out via the Haber Bosch process at elevated pressures of 150 to 250 bar and temperatures of 350 to 500 °C. The hydrogen is obtained via an electrolysis plant, while the nitrogen is supplied from an Air Separation Unit (ASU). To avoid complexities, ASU is not simulated in the process. The flow diagram of the simulated process is shown in the Figure 4.3.

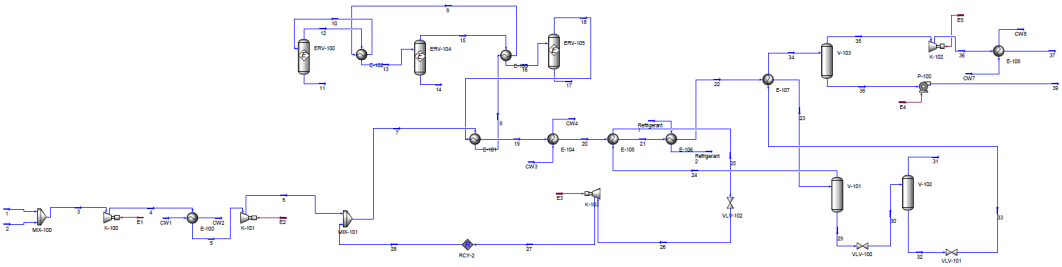

Figure 4.3: Simulated process flow diagram of ammonia synthesis

The Haber Bosch ammonia synthesis is carried out over an iron-based or Ruthenium-based catalyst [63]. Iron catalyst promoted by Al_2O_3, K_2O, CaO, and SiO_2 is reported to have higher per pass ammonia conversion up to 15 to 20 %. The reactor type used for simulation is an equilibrium reactor governed by the following kinetics [40].

$$log_{10}K_a = \beta log_{10}T - 5.519265x10^5 + 1.848863x10^{-7}T^2 + \frac{2001.6}{T} + 2.6899 \qquad (4.1)$$

Where K_a is the equilibrium constant, T is the temperature in Kelvin, and β is the pressure-dependent term, which is considered to be -2.69 for the assumed process conditions [40].

The mixture of hydrogen and nitrogen gas in the molar ratio 3:1 is compressed to 150 bar using a 2-stage compressor. The reactant gas mixture is preheated by exchanging heat with the reactor outlet streams. The reaction mixture enters the 1st reactor bed at 350 °C and 150 bar. The reaction is highly exothermic, and the product stream at the outlet is cooled down by exchanging heat with the reactor inlet stream, before entering the next reactor bed. The product from the outlet of the third reactor bed is cooled and sent to the refrigeration loop, where ammonia is liquified, and the unreacted gas mixture is recycled

back to the synthesis section. The key results from the simulation are summarized in Table 4.2.

Table 4.2: Ammonia synthesis simulation results

	Simulation	Literature	Unit
Conversion per pass	23	17 – 20	%
Overall conversion	99.70	98 - 99	%
Specific Energy Consumption	0.19	0.14	kWh/ kg NH_3

4

METHANOL SYNTHESIS

Reactions considered for methanol production are namely methanol synthesis and reverse water gas shift reaction. The process is carried out in the temperature range of 200 to 270 °C and at 10 to 80 bar. The process is modelled using an equilibrium reactor governed by the equilibrium kinetics in the form:

$$log_{10}K_p = \frac{A}{T} - B \tag{4.2}$$

Where K_p is the equilibrium constant for the respective reaction. Constants A and B for each reaction are shown in Table 4.3.

Table 4.3: Equilibrium coefficients for Methanol synthesis and reverse water gas shift reaction

	A	B
K_{P1}	3066	10.592
K_{P2}	-2073	-2.29

CO_2 gas is compressed at 30 bar in a single-stage reciprocating compressor, and mixed with the hydrogen gas in the molar ratio of 1:3. The reactant gas mixture is further compressed to 55 bar and preheated by the product stream before entering the reactor. The product stream is cooled and condensed to 35 °C, while the unreacted reactants are recycled back to the reactor. A small amount of recycled gas is purged and vented to flare to avoid the accumulation of inerts.

The condensed product stream which contains mostly methanol and water needs to be purified in the distillation column. The distillation column operates at atmospheric pressure and a temperature of 70 °C. Hence, the product stream is expanded via a valve and finally sent to the distillation column after going through a separator. Methanol gas obtained at the top of the distillation column is condensed to obtain the liquified methanol product. The flow diagram of the simulated process is shown in Figure 4.4.

The key results from the simulation are summarized in the following table.

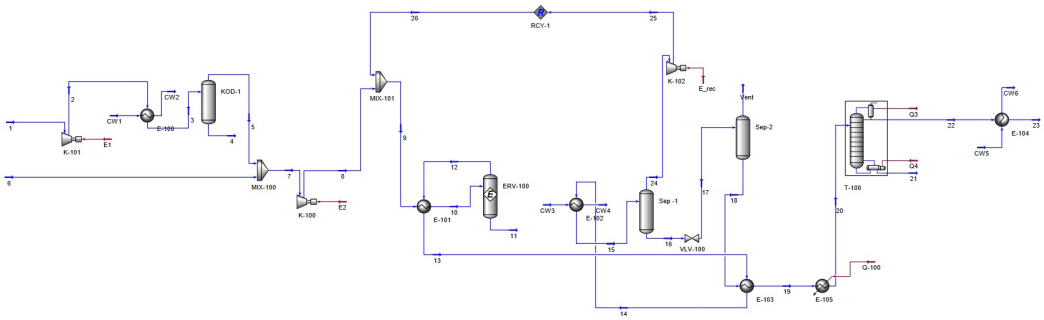

Figure 4.4: Flow diagram of the simulated methanol synthesis process

4

Table 4.4: Methanol synthesis simulations results

	Simulation	Literature	Unit
MeOH purity	99.43	>99	%
Selectivity	72.31	> 70	%
No. of distillation column trays	26	-	#
SEC	0.18	0.16 - 0.21	kWh/ kg MeOH

Ammonia Cracking

At the end of the supply chain, hydrogen gas is obtained from ammonia via the cracking process. The flow diagram of the ammonia cracking process is shown in the Figure 4.5.

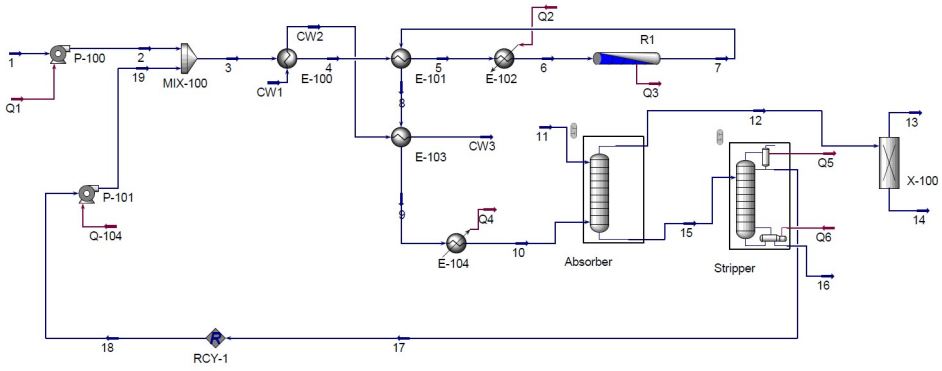

Figure 4.5: Process flow diagram of simulated ammonia cracking process

Ammonia cracking is an endothermic reaction that is carried out at elevated temperatures of 500 to 750 °C and 10 bar pressure. The cracking reaction over Ru/ Al_2O_3 catalyst is governed by the Arrhenius kinetics, with the activation energy of 117 KJ/mol.

$$K = 6x10^{8} exp(\frac{-Ea}{RT}) \tag{4.3}$$

The conversion obtained in the reactor is 97.3 %. The reactor outlet stream is cooled by using a series of heat exchangers and fed to the absorber. Water is fed at the top of the absorber to recover the unreacted ammonia. The absorber operates at 8 bar pressure and 20 °C temperature. The ammonia - free top stream of the absorber is sent to the pressure swing adsorption unit for the separation of hydrogen and nitrogen gases. The bottom stream of the absorber, which mostly consists of ammonia and water, is fed to the stripper for ammonia recovery. The recovered ammonia is pumped and recycled back in the cracking process.

The key results from the ammonia cracking process simulation are summarized in the following table. It should be noted that there is scarce data available regarding the specific energy consumption of the cracking process. However, some of the papers suggest that the energy required to crack ammonia is approximately equal to 15% of the LHV of the product hydrogen (0.80 kWh/ kg NH_3).

Table 4.5: Ammonia cracking simulation results

	Result	Unit
Ammonia conversion	99.30	%
Length of reactor	6	m
Diameter	1.50	m
No. of absorber trays	15	#
SEC	1.37	kWh / kg NH_3

METHANOL REFORMING

Methanol steam reforming is an endothermic reaction, carried out at moderate temperatures of 200 to 300 °C and lower pressures. The reforming reaction is accompanied by unwanted side reactions methanol decomposition and water gas shift reaction. However, it has been reported in the literature that the CO formed by these reactions is less than 1% and hence these reactions can be neglected [7], [48]. Moreover, $Cu/ZnO/Al_2O_3$ catalyst is used in this study, which has higher selectivity towards CO_2. The kinetics of the methanol steam reforming over the said catalyst are expressed in the form of the Arrhenius equation, with an activation energy of 100.9 KJ/mol.

$$K = 1.9x10^{12} exp(\frac{-Ea}{RT}) \tag{4.4}$$

Similar to ammonia cracking, methanol-reforming is also simulated as a membrane reactor system. A mixture of methanol and water is pumped to 10 bar and preheated to 250 °C before entering the reactor. The process flow diagram is shown in the Figure 4.6. The reaction is a highly endothermic reaction. Hence, the temperature of the reactor is maintained at 250 °C by external heating. The reactor outlet stream is used to preheat

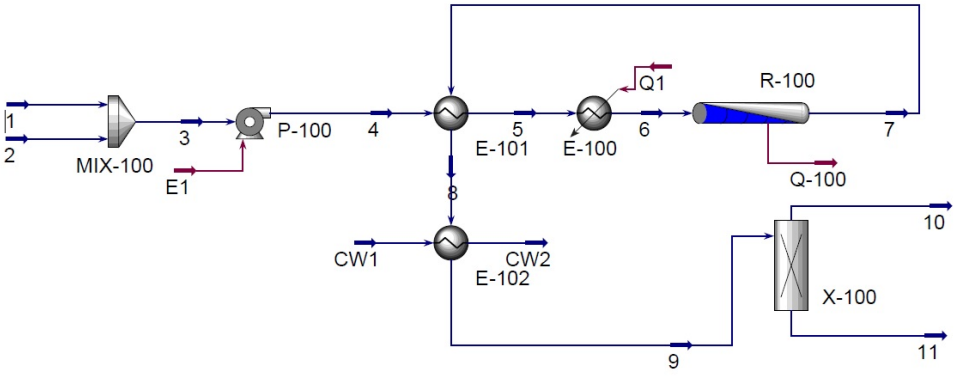

Figure 4.6: Process flow diagram of simulated Methanol reforming process

the reactor inlet stream. Finally, hydrogen and CO_2 gases are separated in the pressure swing adsorption unit to obtain the product H_2. The key results of the simulation are summarized in the following table.

Table 4.6: Methanol reforming simulation results

	Result	Unit
Methanol conversion	100	%
Length of reactor	5	m
Diameter	1.50	m
SEC	1.27	kWh / kg MeOH

Methylcyclohexane - Toluene LOHC system

Toluene hydrogenation

Toluene hydrogenation is an exothermic reaction carried out at a temperature of 250 °C and 8 bar pressure. The storage of hydrogen in the form of LOHCs is a comparatively novel concept, thus little data is available regarding the kinetics of the reactions. Hence, a conversion reactor is used to simulate the toluene hydrogenation process. Toluene conversion is assumed to be 99% [8]. The flow diagram of the simulated process is shown in Figure 4.7.

Toluene is preheated and vaporized in a series of heat exchangers. The vaporized toluene is mixed with the hydrogen gas and fed to the conversion reactor. The product heat is used to preheat the reactants, and it is further cooled to condense the product MCH. The purity of the product MCH is 98.95%.

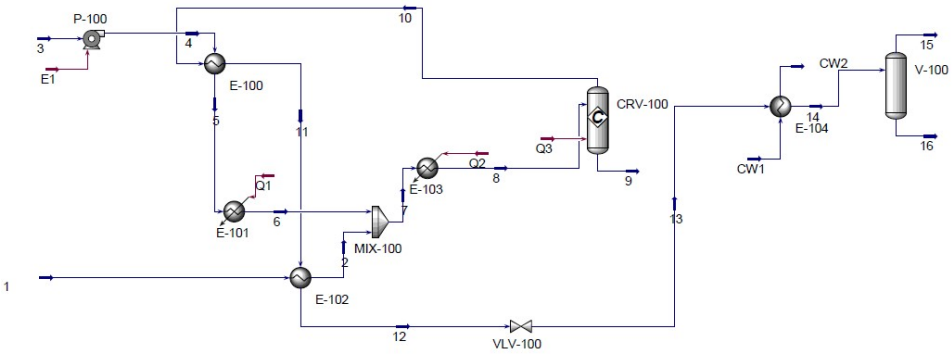

Figure 4.7: Process flow diagram of simulated Toluene hydrogenation process

MCH hydrogenation

MCH dehydrogenation is an endothermic reaction carried out at elevated temperatures of 250 - 450 °C and lower pressures. The reaction is simulated using a conversion reactor, with an MCH conversion of 95% [21]. The flow diagram of the dehydrogenation process is shown in Figure 4.8.

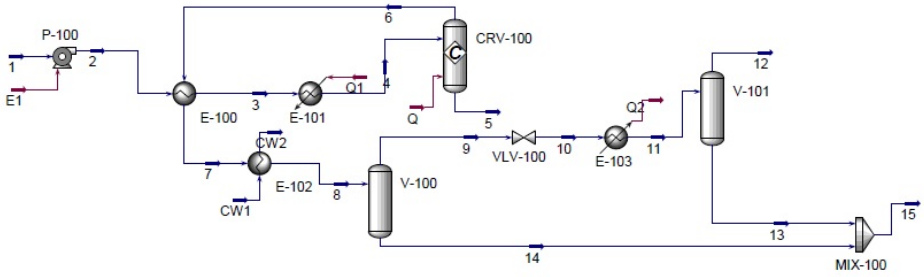

Figure 4.8: Process flow diagram of simulated MCH dehydrogenation process

The feed MCH is pumped to 1.8 bar, preheated, and vaporized in heat exchangers up to 360 °C. The product stream is cooled to separate hydrogen gas and condensed toluene. The purity of toluene is 98.99%, while that of hydrogen is 98.62%. It should be noted that depending on the application of hydrogen gas, it may need to be purified further if purity >99% is required.

DBT - PDBT LOHC SYSTEM

Dibenzyltoluene and Perhydro Dibenzyltoluene are not present in the UniSim Design component list. Hence, two hypothetical components were created using the known critical physicochemical properties of the compounds. The following properties were inserted in UniSim to create the components [65].

Table 4.7: DBT and PDBT critical physicochemical properties

	DBT	PDBT	Unit
Molecular Weight	272.38	290.52	g/mol
Boiling Point	407	355	°C
Density	1040	910	kg/m^3

DBT Hydrogenation

Hydrogenation of DBT is an exothermic reaction carried out at 30 to 100 bar and 80 to 180 °C. Due to the lack of availability of accurate kinetic data for the reaction, a conversion reactor with 99% conversion is used for the simulation [34]. The simulated process flow diagram is shown in Figure 4.9.

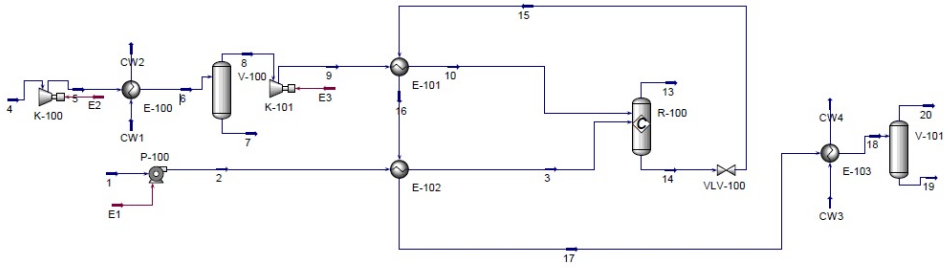

Figure 4.9: Process flow diagram of simulated DBT hydrogenation process

Gaseous hydrogen is compressed to 70 bar and preheated to 170 °C using the reactor outlet stream before entering the reactor. DBT is also pumped to 70 bar, preheated, and finally vaporized before entering the conversion reactor. As the product PDBT is stored at atmospheric pressure, the product stream is depressurized using a valve, and heat is recovered by exchanging with reactant streams. The product is finally condensed in a cooler and sent to a separator, where PDBT is recovered at the bottom. The top stream of the separator consists of hydrogen, which is sent to the flare.

The reaction is exothermic in nature, and about 3 kWh/ kg H_2 heat is released in the overall process. The purity of product PDBT is 98.93 %.

PDBT Dehydrogenation

The dehydrogenation of PDBT is an endothermic reaction, carried out at 240 to 300 °C at 1 to 5 bar pressure. The kinetics of the reaction over a Pd catalyst are represented by the following equation [69]:

$$K = 1.2524 exp(\frac{-Ea}{RT}) C_{PDBT}^{1.98} \tag{4.5}$$

Reactant PDBT is pumped, preheated, and vaporized up to 280 °C. The reaction is carried out in a Plug Flow Reactor. The product stream is condensed in a cooler, and the products DBT and gaseous hydrogen are separated in a separator. The process flow diagram of the simulated process is shown in the Figure 4.10.

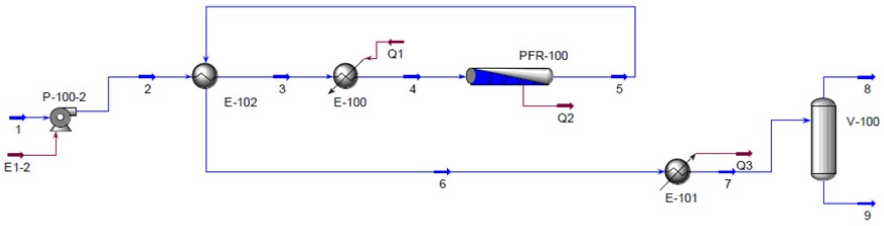

Figure 4.10: Process flow diagram of simulated PDBT dehydrogenation process

A total of 99.23% conversion of PDBT is achieved in the reactor, with an SEC of 4.96 kWh/kg H_2. The purity of product DBT and hydrogen is 99.16 % and 100 % respectively.

5

ECONOMIC ANALYSIS

The cost estimation of engineering projects is divided into multiple classes as per the Association for the Advancement of Cost Estimation International (AACE International) [1]. These classes have a specific range of accuracy associated with them based on their purpose and the degree of project definition variables. In this report, class 4 estimates, also known as preliminary estimates, are carried out for different hydrogen carrier pathways. The accuracy of these estimates is expected to be in between +- 30% range. Cost estimation is based on the guidelines provided in the book "Chemical Engineering Design: Principles, Practice and Economics of Plant and Process Design" [80].

The fixed capital investment cost is calculated for each hydrogen carrier pathway. It consists of the inside battery limits (ISBL) costs, the outside battery limits (OSBL) costs, engineering and construction costs, and contingency costs. To determine these cost components, the factorial method is used, where initially the total purchased equipment cost is determined and remaining cost components are predicted by using various factors. Purchased equipment cost and subsequent estimation of the fixed capital investment is explained in subsequent sections.

Purchased Equipment Costs
The purchased equipment cost is calculated using the following relation:

$$C_e = a + bS^n \tag{5.1}$$

Where, C_e = purchased equipment cost in USD, 2010.
a, b = cost constants
S= sizing parameter for respective equipment
n = exponential term for respective equipment

To calculate the purchased equipment cost, data for the sizing parameter of major equipment is obtained from the UniSim simulations. The sizing data is directly available for the majority of the equipment, with the exceptions of reactors, heat exchangers and

separators. The heat transfer area of the exchangers is determined by "Unisim STE design tool", while the sizing of the separators is done using the McDermott inhouse software. The list of major equipment in the simulations and associated cost assumptions are listed in the Table 5.1 :

Table 5.1: Major equipment with associated cost data [80]

Equipment	Sizing term	Sizing unit	a	b	n
Static mixer	Flow	L/s	570	1170	0.4
Reciprocating compressor	Driver power	kW	260,000	2700	0.75
Shell and tube heat exchanger	Area	m^2	28000	54	1.2
Pressure vessels	Shell mass	kg	11600	34	0.85
Centrifugal pumps	Flow	L/s	8000	240	0.9
Sieve trays	Diameter	m	130	440	1.8

The ISBL costs (C) are given by the equation:

$$C = \sum C_e(1 + f_p + f_{er} + f_i + f_{el} + f_c + f_s + f_l) \tag{5.2}$$

ISBL, OSBL, and other costs The ISBL plant costs consist of procurement and installation of the plant equipment. Once the total purchased equipment cost is determined, the ISBL costs can be determined by using different factors. For fluid handling plants, the factors used for determination of ISBL costs are listed in Table 5.2:

Table 5.2: Factors to determine ISBL costs [80]

Component	Abbreviation	Factor
Piping	f_p	0.8
Equipment Erection	f_{er}	0.3
Instrumentation and control	f_i	0.3
Electrical	f_{el}	0.2
Civil	f_c	0.3
Structures and buidlings	f_s	0.2
Lagging and paint	f_l	0.1

The offsite costs, detailed engineering and design costs, and the contingency costs are typically calculated as a percentage of ISBL costs. Depending on whether the project site is greenfield or brownfield, the offsite costs may vary. The factors used for determination of offsite, engineering, and contingency are listed in the Table 5.3:

Table 5.3: Factors for remaining cost considerations [80]

Component	Abbreviation	Factor
Offsite	OS	0.3
Design and engineering	D&E	0.3
Contingency	X	0.1

Considering the aforementioned factors, the total fixed capital cost C_{FC} is calculated using the formula:

$$C_{FC} = C(1 + OS)(1 + D\&E + X) \tag{5.3}$$

Cost Escalation and currency correction

The basis of cost data for purchased equipment costs is U.S. Gulf Coast, January 2010. Hence, these costs, and any other costs wherever applicable, are escalated to the 2022 cost levels using Chemical Engineering Plant Cost Index.

$$Cost_{2022} = Cost_{2010}(\frac{CEPCI_{2022}}{CEPCI_{2010}}) \tag{5.4}$$

The CEPCI for 2010 is 532.9, while for the year 2022 is 749 [58]. Furthermore, the costs in US$ are converted to euros using the average exchange rate of 0.951 for the year 2022 [31].

Fixed capital investment results

Based on the aforementioned methodology, the fixed capital investment costs for each hydrogen carrier are calculated. The results are summarized in Table 5.4:

Table 5.4: Fixed capital investment costs - results summary

Carrier	M€(2022)
Compressor	16.00
MeOH synthesis	16.97
MeOH reforming	25.67
Ammonia synthesis	26.15
Ammonia cracking	31.01
DBT hydrogenation	9.64
PDBT Dehydrogenation	7.96
Toluene hydrogenation	5.65
MCH Dehydrogenation	16.11
H_2 liquefaction	66.80

An in-depth breakdown of the costs is provided in the Appendix B.

6

RESULTS AND DISCUSSIONS

The total capital investment results obtained in chapter 5 are used in the MATLAB model, as per the methodology explained in chapter 3 to obtain the final results. The LCOH results of all the hydrogen carrier chains for each of the four routes taken into consideration in this study are summarized in Table 6.1. It should be noted that hydrogen production via electrolysis is not included in the scope of study, hence the LCOH values are excluding the cost of hydrogen production. The highest LCOH is found in supply networks utilizing compressed hydrogen gas, while the lowest is for the ammonia chains, making them the most economical option. From the table, it can be seen that except for compressed hydrogen chains, there is not much of difference in the LCOH of the carriers amongst different routes. Moreover, the trend of the LCOH results, is the same across all the routes. A detailed interpretation of the results is carried out in the following sections.

Table 6.1: LCOH results for the selected routes

	Australia to Japan	Chile to USA	Egypt to the Netherlands	Saudi Arabia to Germany
Carrier	LCOH (€/ kg H_2)			
CGH_2- chain 1	27.43	40.38	22.14	29.81
CGH_2 - chain 2	27.57	40.48	22.23	29.94
LH_2	9.32	9.31	8.39	9.31
NH_3 - chain 1	2.23	2.25	2.22	2.23
NH_3 - chain 2	2.24	2.27	2.22	2.24
MeOH	2.33	2.43	2.26	2.35
DBT	2.83	2.80	2.80	2.82
Toluene	3.75	3.72	3.71	3.74

ANALYSIS OF COMPRESSED HYDROGEN GAS CHAIN

As mentioned earlier, the supply networks utilizing compressed hydrogen gas have the highest LCOH. This can be explained by the requirement for intermediate booster compressor stations to maintain the necessary hydrogen pressure over longer distances. Moreover, installation of new pieplies or modification of existing natural gas pipelines also has a higher upfront cost. Thus, the increased LCOH results from increased capital expenditures for long distance pipelines, booster compressor units, as well as their increased energy needs. It should be highlighted that these findings apply to the scenario in which existing natural gas pipelines that repurposed to transport hydrogen are taken into account. The installation of new pipelines resulted in a LCOH of compressed gas supply chains above 180 (€ / kg H_2) for all the routes. It can be concluded that transport of hydrogen in the form of compressed gas is not economical for long distances overseas.

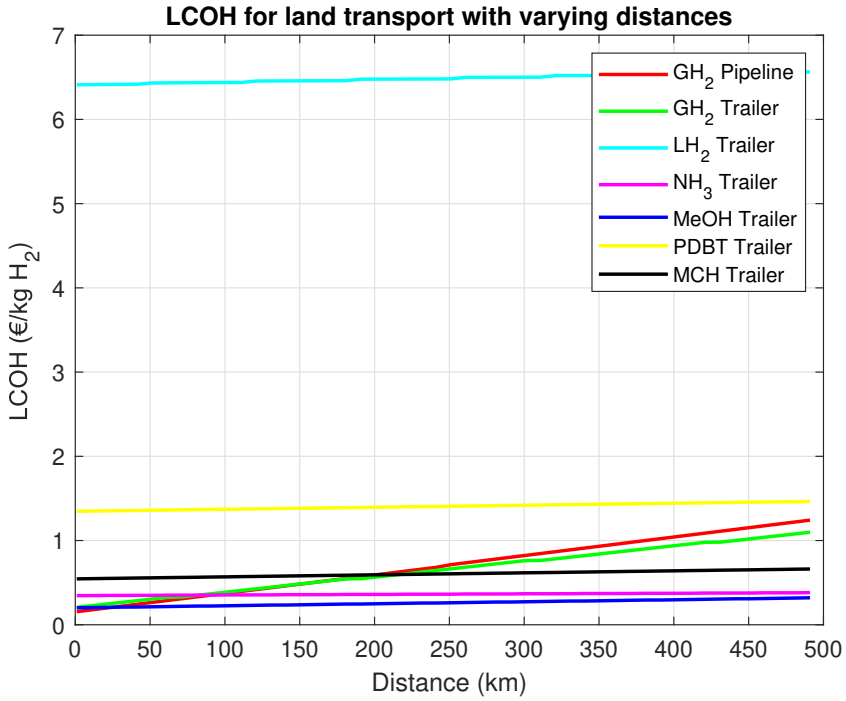

Figure 6.1: LCOH for land transport with varying distances

However, compressed hydrogen gas could be regarded as competitive with the other carriers for shorter distances over land. A sensitivity study for LCOH of carriers' distribution chains with various distances is shown in the Figure 6.1. Transporting compressed hydrogen gas through pipelines and tube trailers is less expensive over all distances than converting it to liquid hydrogen and transporting it in that form. Additionally, the compressed hydrogen alternative can be more cost-effective than some other carriers,

depending on the distance. Again, it should be noted that these results are for the scenario with the repurposed natural gas pipelines, and that for this result to be true, the natural gas pipelines must already exist in the pathway under consideration. Thus, it may be concluded that the transportation of hydrogen in the form of compressed hydrogen is practical for short distances over land, but should be assessed on a case-by-case basis.

Analysis of Liquid Hydrogen Chain

Out of the remaining pathways, hydrogen liquefaction has the highest LCOH. Figure 6.2 depicts the breakdown of the liquid hydrogen chain. The cost of liquefying hydrogen accounts for 69% of the LCOH in the liquid hydrogen chain. The adjacent pie chart displays the breakdown of costs in the liquefaction unit. It is clear that the cost of refrigerant nitrogen is the major factor. This is due to the fact that the nitrogen refrigeration cycle is not modelled in this analysis. Instead, it is assumed that a nearby air separation unit provides the liquid nitrogen. As a result, after being utilized in the system, the gaseous nitrogen is sent to the stack rather than being recirculated. However, refrigeration and recycling of the nitrogen can result in a substantial decrease in the hydrogen liquefaction costs. That, in turn, will reduce the LCOH of the liquid hydrogen chain.

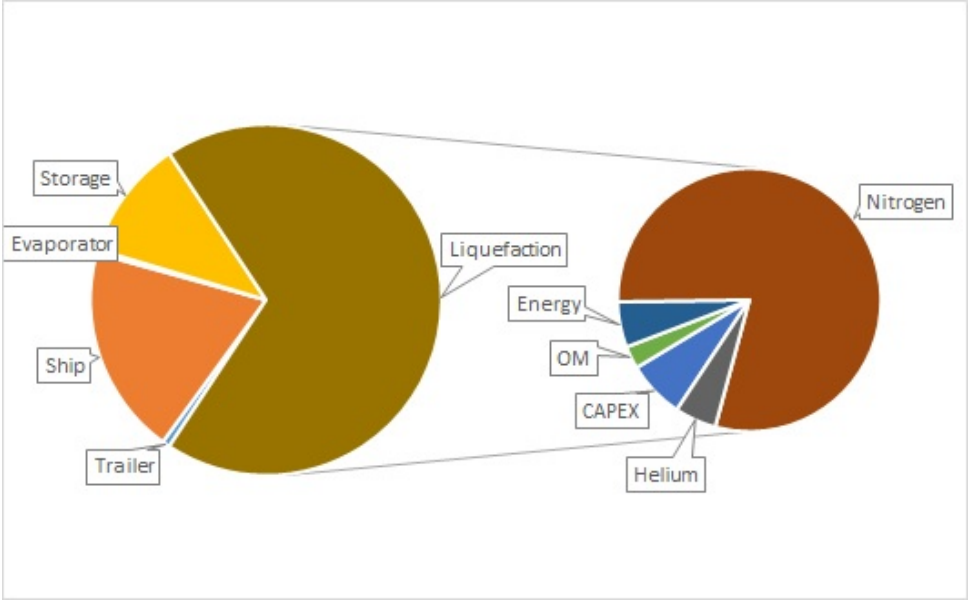

Figure 6.2: LCOH breakdown for LH_2 chain

Additionally, the capacity of liquid hydrogen ships considered in this analysis is 1250 m3. However, Kawasaki Heavy Industries have received an Approval in Principle for the design of a cargo containment system capable of storing the highest capacity in the world. This system will have a capacity of 40,000 m3 per tank and is designed for deployment on a

huge liquefied hydrogen carrier. Considering this, liquid hydrogen has the potential to become a more competitive carrier as compared to other options in the near future.

ANALYSIS OF DEHYDROGENATION PROCESSES

For the other carriers, the predominant element of the corresponding LCOH is dehydrogenation or conversion of the carrier back to hydrogen at the end of the supply chain. The breakdown of the dehydrogenation component for these carriers is depicted in a stacked plot in the Figure 6.3.

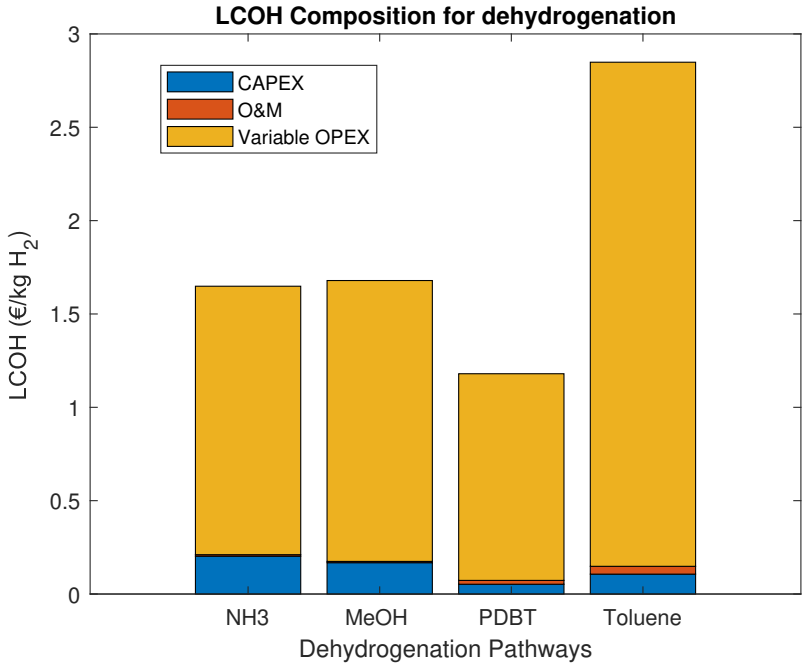

Figure 6.3: LCOH breakdown for dehydrogenation processes

With its contribution varying between 85 and 95 percent for various paths, it is evident that the variable OPEX is the prominent component. Since the dehydrogenation reactions are endothermic in nature, they are more favorable at higher temperatures. Additionally, it is necessary to provide external heating by means of fired heaters, in order to sustain the reaction temperatures. The higher variable OPEX corresponds to the costs associated with natural gas, which is used as a fuel in the fired heaters. Electrification of the dehydrogenation processes could lead to a reduction in the variable OPEX, which will be explored later in the chapter.

Round trip efficiency

The energy consumption percentage for each step of the supply chain, considering the lower heating value (LHV) of hydrogen, is computed for all hydrogen vectors in Table 6.2. The highest round trip efficiency is observed for compressed hydrogen chains, while lowest for tolune - MCH chain. Except for compressed and liquefied hydrogen, the dehydrogenation step incurs the highest efficiency loss in all other hydrogen vectors due to higher energy consumption. Considering this, it would be advantageous to utilize these vectors in their original form for other applications rather than converting them back into hydrogen.

Table 6.2: Energy consumption and round trip efficiencies

	Hydrogenation	Distribution	Transmission	Dehydrogenation	Round trip efficiency
CGH_2- 1	3.14%	0.00%	2.48%	0.00%	94%
CGH_2- 2	3.14%	0.58%	2.48%	0.00%	94%
LH_2	26.79%	0.07%	4.47%	1.80%	67%
NH_3-1	4.11%	0.10%	7.96%	19.32%	69%
NH_3-2	4.11%	0.10%	3.72%	19.32%	73%
MeOH	2.82%	0.31%	0.62%	20.22%	76%
DBT	1.32%	0.86%	1.54%	14.88%	81%
Toluene	2.82%	0.92%	1.85%	36.30%	58%

Sensitivity with increasing electrolyzer size

The sensitivity analysis for the scenario where the size of the hydrogen electrolyzer is increased from 100 MW to 1000 MW is shown in the Figure 6.4. Since the hydrogen output from the electrolyzer unit serves as the basis or input for all the carriers, the corresponding plant sizes will consequently change.

Since there are no current natural gas pipeline networks connecting the countries taken into account in this study, new pipes are considered for the transportation of compressed hydrogen for sensitivity analysis. Moreover, one of the user inputs in the model is pipeline diameter, which ranges from 20 to 48 inches. For the purpose of this sensitivity analysis, the pipeline size has been set to be 48 inches. There is a significant reduction in the LCOH for the compressed gas pathway from 187 (€ / kg H_2) for 100 MW plant to 19 (€ / kg H_2) for 1000 MW plant. However, it is still considerably higher when compared to other carriers.

It is evident from the figure that all of these pathways' LCOH decreases as plant size increases. This comes as no surprise because the model takes economies of scale into account. However, the decline is not consistent throughout the sizes; rather, there are certain intermediate peaks where the LCOH rises for a particular plant size before decreasing again subsequently. When specific supply chain components were examined,

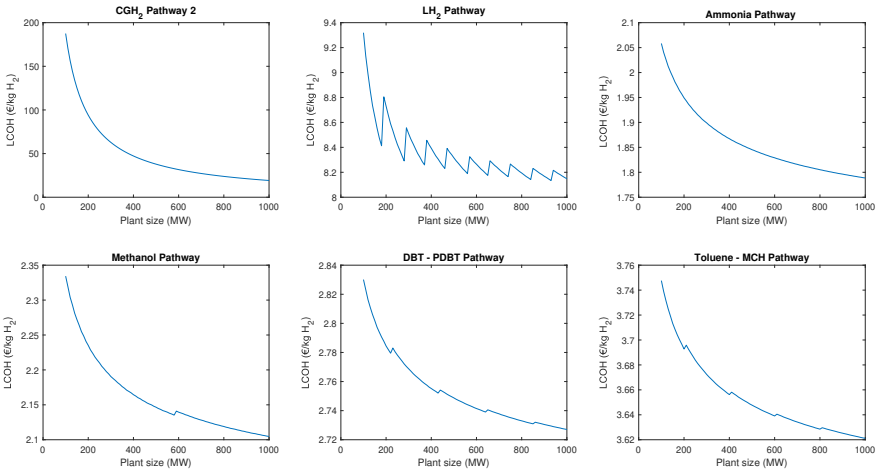

Figure 6.4: Change in LCOH with changing the size of the electrolyzer

6

the cost of overseas shipping was found to be the main driver behind the increase. This is due to the fact that one carrier ship is insufficient to transport the respective carrier continuously without any interruptions after a certain increase in plant size. Thus, the CAPEX of the additional ship, as well as the fuel consumption, is reflected in the increased peak. Since the capacity of liquid hydrogen ship is lower (1050 m^3) as compared to other carriers, it results in increased frequency of the peaks for the liquid hydrogen pathway. Similarly, the cases where the size of the carrier ship is greater, have lower frequency of the peaks.

CO_2 EMISSIONS

The annual CO_2 emissions for the Australia to Japan route are summarized in Table 6.3. Since only the scope 1 emissions are considered, and the compressed hydrogen chain 1 consists of pipelines for both transport on land and the sea, it does not have any direct CO_2 emissions. For the 2nd compressed hydrogen chain, there are significant emissions from the land support, since the payload of the compressed hydrogen tube trailers is lower as compared to other carriers, consequently requiring a higher number of tube trailers to transport the hydrogen.

For ammonia chains, the only difference is the size of the carrier ship. For chain 1 MGC is considered that has a capacity of 35000 m^3, while for case 2 LGC is considered with a capacity of 59000 m^3. From previous results, it was shown that there is not much impact on the LCOH of these chains, however, for CO_2 emissions considerations, the use of LGC is preferable since it has 46 % lower emissions in the sea transport at as compared to the MGC chain.

Table 6.3: Annual CO_2 emissions and associated costs

	Annual CO_2 emissions (Tons / year)				CO_2 credit costs
Carrier	Land transport	Sea transport	Dehydro	Total	(M €/year)
CGH_2 - chain 1	0	0	0	0	0.00
CGH_2 - chain 2	7761	0	0	7761	0.71
LH_2	1358	8236	0	9594	0.87
NH_3 - chain 1	1552	14614	22567	38733	3.52
NH_3 - chain 2	1552	6818	22567	30937	2.81
MeOH	6687	1135	23876	31698	2.88
DBT	20060	2838	17322	40220	3.66
Toluene	20060	3406	42067	65532	5.96

Toluene - MCH chain has the highest annual CO_2 emissions due to the emissions from dehydrogenation process. Dehydrogenation of MCH has the highest specific energy consumption of 12 kWh/kg H_2 as compared to other carriers, which is fulfilled by the fired heaters. Usage of natural gas in the fired heaters translates into higher CO_2 emissions for the toluene- MCH chain. Moreover, DBT and toluene have lower hydrogen storage capacity on wt. % basis as compared to methanol, leading to a higher number of tanker requirements to transport the same quantity of hydrogen. This effect is also reflected in the higher CO_2 emissions for DBT and toluene chains for land transport.

From the table, it is clear that none of the feasible options are entirely green when CO_2 emissions are considered. Since the long haul transport sector is considered to be a hard sector for CO_2 abatement, the CO_2 emissions could be reduced by electrifying the dehydrogenation part. The effect of electrifying the dehydrogenation process on the LCOH and CO_2 emissions will be analyzed in the following section.

Electrification

In the base case, it was considered that the heating requirements in the process plants will be fulfilled by the fired heaters. Table 6.4 summarizes the results for the case, where heating is provided by electric heaters. Thus, the cost of fuel consumption is replaced by the cost of corresponding electricity consumption. Moreover, the total installed cost of the electric heaters for different power ratings is determined using McDermott in-house data.

Table 6.4: Reduction in CO_2 emissions after electrification

Carrier	Initial emissions (Ton/year)	Emissions after electrification (Ton/year)	% reduction
CGH_2- chain 1	0	0	0
CGH_2 - chain 2	7761	7761	0
LH_2	9594	9594	0
NH_3 - chain 1	38733	16166	58.26
NH_3 - chain 2	30937	8370	72.94
MeOH	31698	7822	75.32
DBT	40220	22898	43.07
Toluene	65532	23465	64.19

The data shows that electrification may significantly reduce CO_2 emissions, with as much as a 75% reduction in methanol systems. Since the variable OPEX dominates the LCOH, replacing fired heaters with electric heaters results in a sizable reduction in LCOH even though the cost of electric heaters is about twice as high as the cost of fired heaters of equal rating. The highest LCOH reduction of 64 % is achieved in the toluene - MCH system, followed by 60 % in both ammonia chains. There is a LCOH reduction of 50 and 30 % in the methanol and DBT pathways respectively. Ultimately, as far as LCOH is concerned, ammonia chains come out at the top.

Table 6.5: Reduction in LCOH after electrification

Carrier	LCOH - base case (€/kg H_2)	LCOH - after electrification (€/kg H_2)	% Reduction
CGH_2- chain 1	27.43	27.43	0.0
CGH_2 - chain 2	27.32	27.32	0.0
LH_2	9.32	9.32	0.0
NH_3 - chain 1	2.23	0.89	60.2
NH_3 - chain 2	2.24	0.90	59.9
MeOH	2.33	1.16	50.3
DBT	2.83	1.98	30.1
Toluene	3.75	1.36	63.7

Model limitations and recommendations

The scope of this report is limited to analyzing the supply chain of hydrogen, specifically after the production stage, while excluding hydrogen production via electrolysis. To fully understand the entire chain from manufacturing to final utilization, hydrogen production must be taken into consideration. The LCOH for hydrogen can be heavily influenced by variables including the type and efficiency of the electrolyzer used, as well as the renewable energy sources used to generate electricity. Thus, in future studies, it is recommended to include hydrogen production as well.

Additionally, a continuous supply of hydrogen is assumed as the input to the model. However, as far as green hydrogen is considered, the production is far from continuous due to the intermittency of renewable energy. Consequently, that will affect the production of the hydrogen carrier, and in turn the entire supply chain. To account for this, minimum and maximum production rates (as a % of respective capacities), and ramp-up / ramp-down rates need to be included to make the model robust.

Moreover, use of the gaseous hydrogen or other carriers such as ammonia, and methanol as a source of fuel for trailers and ships in their respective supply chains in the analysis could be an interesting idea. Additionally, they can also be used as fuel in the fired heaters to fulfill the heating requirements in the dehydrogenation processes. Although it will decrease the amount of hydrogen delivered throughout the chain, it will assist in lowering CO_2 emissions.

In this analysis, tankers made of stainless steel that operate at 200 bar are taken into account for the transportation of compressed hydrogen gas. New tankers made of composite materials, however, have larger hydrogen payload capacity. Some of these vessels can transport up to 1100 kg of hydrogen, which is a significant advancement over the tankers taken into account in this study. However, in these tankers, the hydrogen is stored at higher pressures of up to 350 barg. Therefore, more energy is needed for compression, which increases both the CAPEX and OPEX of the system. Thus, this trade-off needs to be analyzed further.

Finally, one of the elements missing from these supply chains is loading-unloading terminals for the carriers. The costs and energy requirements for the terminals could help in improving the model.

7

Conclusions

In this report, multiple promising hydrogen vectors were analyzed for the storage and transportation of hydrogen. A MATLAB model was built to determine the LCOH of the entire supply chain for each hydrogen vector. The model's findings show that supply networks using compressed hydrogen gas have the highest LCOH, whereas ammonia chains have the lowest. Furthermore, the LCOH of the carriers along various transportation routes does not differ significantly, except for compressed hydrogen gas chains.

While it is not cost-effective to transport hydrogen in the form of compressed gas over longer distances overseas, it is competitive with alternative methods over shorter distances on land. The second largest LCOH is found in liquid hydrogen chains, behind compressed hydrogen gas. It is discovered that higher LCOH is caused by the price of liquid nitrogen, which serves as a refrigerant in the process of liquefying hydrogen. In addition, it is concluded that given major capacity improvements in large scale liquid hydrogen carrier vessels, liquid hydrogen could be a potential carrier in the near future.

Dehydrogenation, or converting the carrier back to hydrogen at the final step of the supply chain, is the dominant component of the LCOH for the remaining carriers. Because the dehydrogenation reactions are endothermic in nature, external heating must be provided using fired heaters in order to maintain the reaction temperatures, which in turn influences the LCOH.

CO_2 emission analysis showed that none of the supply chains are entirely green, with the toluene-MCH chain having the highest annual CO_2 emissions. However, the emissions can be greatly reduced by electrifying the dehydrogenation processes. Additionally, it results in a substantial reduction in LCOH, with the toluene-MCH chain showing a decline of up to 64%.

In conclusion, this model was successful in presenting a techno-economic overview of promising hydrogen storage and transportation vectors. However, it is suggested to

include the hydrogen production from electrolyzer, to complete the entire value chain. Furthermore, it would be interesting to examine the impact on CO_2 emissions of using hydrogen and other carriers as fuel in their respective supply chains. Finally, inclusion of the costs associated with loading unloading terminals will also help in making the model more robust.

BIBLIOGRAPHY

[1] AACE International. (2020). Cost estimate classification system- as applied in engineering, procurement, and construction for the process industries. https://web.aacei.org/docs. Accessed on May 26, 2023.

[2] Aakko-Saksa, P. T., Cook, C., Kiviaho, J., and Repo, T. (2018). Liquid organic hydrogen carriers for transportation and storing of renewable energy – review and discussion. *Journal of Power Sources*, 396:803–823.

[3] Abdin, Z., Tang, C., Liu, Y., and Catchpole, K. (2021). Large-scale stationary hydrogen storage via liquid organic hydrogen carriers. *iScience*, 24(9):102966.

[4] Ablondi, Timothy ; Barton, M. (2022). Compressors are hydrogen 'colour blind'. www.compressortech2.com. Accessed on December 23, 2022.

[5] ACER (2021). *Transporting Pure Hydrogen by Repurposing Existing Gas Infrastructure: Overview of existing studies and reflections on the conditions for repurposing.* European Union Agency for the Cooperation of Energy Regulators.

[6] Acker, M. (2021). Pipeline transportation of ammonia – helping to bridge the gap to a carbon free future. https://www.ammoniaenergy.org/paper. Accessed on June 11, 2023.

[7] Agrell, J., Birgersson, H., and Boutonnet, M. (2002). Steam reforming of methanol over a cu/zno/al2o3 catalyst: kinetic analysis and strategies for suppression of co formation. *Journal of Power Sources*, 106(1):249–257. Proceedings of the Seventh Grove Fuel Cell Symposium.

[8] Akram, M. S. and Usman, M. R. (2021). Simulation and optimization of hydrogen fueled mobile power plant based on methylcyclohexane–toluene–hydrogen cycle. *Theoretical Foundations of Chemical Engineering*, 55:545 – 561.

[9] Ali, A., Kumar, G. U., and Lee, H. J. (2021). Investigation of hydrogenation of dibenzyltoluene as liquid organic hydrogen carrier. *Materials Today: Proceedings*, 45:1123–1127. International Conference on Advances in Materials Research - 2019.

[10] Aslam, R., Khan, M. H., Ishaq, M., and Müller, K. (2018). Thermophysical studies of dibenzyltoluene and its partially and fully hydrogenated derivatives. *Journal of Chemical & Engineering Data*, 63(12):4580–4587.

[11] Aziz, M. (2021). Liquid hydrogen: A review on liquefaction, storage, transportation, and safety. *Energies*, 14(18).

[12] Aziz, M., Wijayanta, A., and Nandiyanto, A. (2020). Ammonia as effective hydrogen storage: A review on production, storage and utilization. *Energies*, 13:3062.

[13] Barron, R. F. (1985). *Cryogenic Systems*. Monographs on Cryogenics. Oxford University Press, New York, NY, 2 edition.

[14] Bettenhausen, C. (2022). Green methanol gains traction. https://cen.acs.org/business/Green-methanol-gains-traction/100/i39. Accessed on May 06, 2023.

[15] Bi, Y. and Ju, Y. (2022). Design and analysis of an efficient hydrogen liquefaction process based on helium reverse brayton cycle integrating with steam methane reforming and liquefied natural gas cold energy utilization. *Energy*, 252:124047.

[16] Blain, L. (2022). Methanol as fuel: An accessible early step toward clean shipping. https://newatlas.com/energy/methanol-fuel-shipping/. Accessed on June 11, 2023.

[17] Brown, T. (2017). Round-trip efficiency of ammonia as a renewable energy transportation media. https://www.ammoniaenergy.org/articles. Accessed on May 1, 2023.

[18] Brun, K. and Simons, S. (2021). Compressor options for the hydrogen economy. www.gascompressionmagazine.com. Accessed on May 19, 2023.

[19] Byun, M., Lee, B., Lee, H., Jung, S., Ji, H., and Lim, H. (2020). Techno-economic and environmental assessment of methanol steam reforming for h2 production at various scales. *International Journal of Hydrogen Energy*, 45(46):24146–24158.

[20] Castello, P., Tzimas, E., Moretto, P., and Peteves, S. D. (2005). Techno-economic assessment of hydrogen transmission and distribution systems in europe in the medium and long term.

[21] Chiyoda Corporation (2017). Spera hydrogen process. https://www.mofa.go.jp/files/000355890.pdf. Accessed on April 26, 2023.

[22] Collins, L. (2022). 'intolerable risk': Methanol winning the hydrogen shipping race as new studies highlight dangers of ammonia at sea. https://www.rechargenews.com/energy-transition/. Accessed on March 19, 2023.

[23] Cui, X., Kær, S. K., and Nielsen, M. P. (2022). Energy analysis and surrogate modeling for the green methanol production under dynamic operating conditions. *Fuel*, 307:121924.

[24] Department of Health (2004). The facts about ammonia. https://www.health.ny.gov/environmental/emergency/chemical_terrorism/ammonia_tech.htm. Accessed on December 22, 2022.

[25] Devitt, P. (2022). How un plan for russian ammonia export could help global fertiliser market. https://www.reuters.com/markets/commodities. Accessed on April 27, 2023.

[26] Devkota, S. (2023). Storage potential of green hydrogen | researchgate. https://www.researchgate.net/post/Storage_Potential_of_Green_Hydrogen. Accessed on February 02, 2023.

[27] Dewar, J. (1898). Preliminary note on the liquefaction of hydrogen and helium. *Science*, 8(183):3–5.

[28] Dodds, P. E. and Demoullin, S. (2013). Conversion of the uk gas system to transport hydrogen. *International Journal of Hydrogen Energy*, 38(18):7189–7200.

[29] European Technology Platform for Zero Emission Fossil Fuel Power Plants (2011). The costs of co2 transport: post-demonstration ccs in the eu. https://www.globalccsinstitute.com/archive/hub/publications/119811. Accessed on May 17, 2023.

[30] European Union (1996). Council directive 96/53/ec. https://eur-lex.europa.eu/legal-content/EN/TXT/?uri=CELEX:31996L0053. Accessed on May 06, 2023.

[31] Exchange Rates UK (2023). Us dollar to euro spot exchange rates for 2022. https://www.exchangerates.org.uk/USD-EUR-spot-exchange-rates-history-2022.html. Accessed on May 25, 2023.

[32] Fuel Cells Works (2023). Calvera hydrogen develops the largest ever hydrogen transport tube trailer model for shell hydrogen. https://fuelcellsworks.com/news/. Accessed on March 24, 2023.

[33] Garcia, G., Arriola, E., Chen, W.-H., and De Luna, M. D. (2021). A comprehensive review of hydrogen production from methanol thermochemical conversion for sustainability. *Energy*, 217:119384.

[34] Garidzirai, R., Modisha, P., Shuro, I., Visagie, J., van Helden, P., and Bessarabov, D. (2021). The effect of mg and zn dopants on pt/al2o3 for the dehydrogenation of perhydrodibenzyltoluene. *Catalysts*, 11(4).

[35] Geng, J. and Sun, H. (2023). Optimization and analysis of a hydrogen liquefaction process: Energy, exergy, economic, and uncertainty quantification analysis. *Energy*, 262:125410.

[36] Gillette, J. L. and Kolpa, R. L. (2007). Overview of interstate hydrogen pipeline systems. http://www.osti.gov/bridge. Accessed on February 03, 2023.

[37] Graf, M. (2021). Costs and energy efficiency of long-distance hydrogen transport options. Master's thesis, University of Natural Resources and Life Sciences, Vienna. Available at https://boku.ac.at/en/bib/.

[38] Gu, Y., Wang, D., Chen, Q., and Tang, Z. (2022). Techno-economic analysis of green methanol plant with optimal design of renewable hydrogen production: A case study in china. *International Journal of Hydrogen Energy*, 47(8):5085–5100.

[39] HESC (2022). Successful completion of the hesc pilot project. https://www.hydrogenenergysupplychain.com/report. Accessed on January 21, 2023.

[40] Humphreys, J., Lan, R., and Tao, S. (2021). Development and recent progress on ammonia synthesis catalysts for haber–bosch process. *Advanced Energy and Sustainability Research*, 2(1):2000043.

[41] IEA (2019). https://www.iea.org/reports/the-future-of-hydrogen, title=The future of green hydrogen. Accessed on January 07, 2023.

[42] IEA (2021). Ammonia technology roadmap. https://www.iea.org/reports/ammonia-technology-roadmap. Accessed on January 19, 2023.

[43] IRENA (2020). Green hydrogen cost reduction. https://www.irena.org/publications/2020/Dec/Green-hydrogen-cost-reduction. Accessed on December 22, 2022.

[44] IRENA (2022a). Global hydrogen trade to meet the 1.5°c climate goal. https://www.irena.org/publications/2022/Jul/Global-Hydrogen-Trade-Outlook. Accessed on January 31, 2023.

[45] IRENA (2022b). Renewable energy statistics 2022. https://www.irena.org/publications/2022/Jul/Renewable-Energy-Statistics-2022. Accessed on December 20, 2022.

[46] IRENA (2022c). World energy transitions outlook 2022: 1.5°c pathway. https://www.irena.org/Energy-Transition/Outlook. Accessed on January 07, 2023.

[47] Jansen, G. (2021). Compressed hydrogen storage. https://energy.nl/data/compressed-hydrogen-storage/. Accessed on February 02, 2023.

[48] Jiang, C., Trimm, D., Wainwright, M., and Cant, N. (1993). Kinetic mechanism for the reaction between methanol and water over a cu-zno-al2o3 catalyst. *Applied Catalysis A: General*, 97(2):145–158.

[49] Jorschick, H., Geißelbrecht, M., Eßl, M., Preuster, P., Bösmann, A., and Wasserscheid, P. (2020). Benzyltoluene/dibenzyltoluene-based mixtures as suitable liquid organic hydrogen carrier systems for low temperature applications. *International Journal of Hydrogen Energy*, 45(29):14897–14906.

[50] Kawasaki (2019). World's first liquefied hydrogen carrier suiso frontier launches building an international hydrogen energy supply chain aimed at carbon-free society. Accessed on February 14, 2023.

[51] Khan, M. A., Cameron, Y., Mackinnon, C., and Layze, D. B. (2021). The techno-economics of hydrogen compression. https://transitionaccelerator.ca/techbrief-techno-economics-hydrogen-compression/. Accessed on January 11, 2023.

[52] Kim, S., Yun, S.-W., Lee, B., Heo, J., Kim, K., Kim, Y.-T., and Lim, H. (2019). Steam reforming of methanol for ultra-pure h2 production in a membrane reactor: Techno-economic analysis. *International Journal of Hydrogen Energy*, 44(4):2330–2339. The 2nd International Conference on Alternative Fuels and Energy (ICAFE2017).

[53] Krasae-in, S., Stang, J. H., and Neksa, P. (2010a). Development of large-scale hydrogen liquefaction processes from 1898 to 2009. *International Journal of Hydrogen Energy*, 35(10):4524–4533. Novel Hydrogen Production Technologies and Applications.

[54] Krasae-in, S., Stang, J. H., and Neksa, P. (2010b). Exergy analysis on the simulation of a small-scale hydrogen liquefaction test rig with a multi-component refrigerant refrigeration system. *International Journal of Hydrogen Energy*, 35(15):8030–8042. The 10th Chinese Hydrogen Energy Conference.

[55] Luo, Z., Hu, Y., Xu, H., Gao, D., and Li, W. (2020). Cost-economic analysis of hydrogen for china's fuel cell transportation field. *Energies*, 13(24).

[56] Makhloufi, C. and Kezibri, N. (2021). Large-scale decomposition of green ammonia for pure hydrogen production. *International Journal of Hydrogen Energy*, 46(70):34777–34787.

[57] Makridis, S. S. (2016). Hydrogen storage and compression. In *Methane and Hydrogen for Energy Storage*, pages 1–28. Institution of Engineering and Technology.

[58] Maxwell, C. (2020). Chemical engineering plant cost index (cepci). https://toweringskills.com/financial-analysis/cost-indices/. Accessed on May 02, 2023.

[59] Melaina, M. W., Antonia, O., and Penev, M. (2013). Blending hydrogen into natural gas pipeline networks: A review of key issues. Technical report, National Renewable Energy Laboratory.

[60] Mintz, M., Gillette, J., Elgowainy, A., Paster, M., Ringer, M., Brown, D., and Li, J. (2006). Hydrogen delivery scenario analysis model for hydrogen distribution options. *Transportation Research Record*, 1983:114–120.

[61] Naik, B. (2022). Honeywell's unisim design suite. https://hcenews.honeywell.com/unisim-design-free-trial. Accessed on June 18, 2023.

[62] Nayak-Luke, R., Forbes, C., Cesaro, Z., Bañares-Alcántara, R., and Rouwenhorst, K. (2021). Chapter 8 - techno-economic aspects of production, storage and distribution of ammonia. In Valera-Medina, A. and Banares-Alcantara, R., editors, *Techno-Economic Challenges of Green Ammonia as an Energy Vector*, pages 191–207. Academic Press.

[63] Nelson, A. E. (2008). Fundamentals of industrial catalytic processes. *The Canadian Journal of Chemical Engineering*, 85(1):127–128.

[64] Newsletters, R. (2008). Ammonia trades fertilised by growing agricultural output. https://www.rivieramm.com/news-content-hub/news-content-hub/ammonia-trades-fertilised-by-growing-agricultural-output-52016. Accessed on January 25, 2023.

[65] Niermann, M., Beckendorff, A., Kaltschmitt, M., and Bonhoff, K. (2019). Liquid organic hydrogen carrier (lohc) – assessment based on chemical and economic properties. *International Journal of Hydrogen Energy*, 44(13):6631–6654.

[66] Niermann, M., Timmerberg, S., Drünert, S., and Kaltschmitt, M. (2021). Liquid organic hydrogen carriers and alternatives for international transport of renewable hydrogen. *Renewable and Sustainable Energy Reviews*, 135:110171.

[67] Office of Energy Efficiency & Renewable Energy (2021). Hydrogen tube trailers. https://www.energy.gov/eere/fuelcells/hydrogen-tube-trailers. Accessed on February 14, 2023.

[68] Papadias, D. D., Peng, J.-K., and Ahluwalia, R. K. (2021). Hydrogen carriers: Production, transmission, decomposition, and storage. *International Journal of Hydrogen Energy*, 46(47):24169–24189.

[69] Peters, R., Deja, R., Fang, Q., Nguyen, V. N., Preuster, P., Blum, L., Wasserscheid, P., and Stolten, D. (2019). A solid oxide fuel cell operating on liquid organic hydrogen carrier-based hydrogen – a kinetic model of the hydrogen release unit and system performance. *International Journal of Hydrogen Energy*, 44(26):13794–13806.

[70] Riaz, A., Qyyum, M. A., Hussain, A., and Lee, M. (2022). Significance of ortho-para hydrogen conversion in the performance of hydrogen liquefaction process. *International Journal of Hydrogen Energy*.

[71] Rouwenhorst, K., Elishav, O., Mosevitzky Lis, B., Grader, G., Mounaïm-Rousselle, C., Roldan, A., and Valera-Medina, A. (2021). Chapter 13 - future trends. In Valera-Medina, A. and Banares-Alcantara, R., editors, *Techno-Economic Challenges of Green Ammonia as an Energy Vector*, pages 303–319. Academic Press.

[72] Sagel, V. N., Rouwenhorst, K. H., and Faria, J. A. (2022). Green ammonia enables sustainable energy production in small island developing states: A case study on the island of curaçao. *Renewable and Sustainable Energy Reviews*, 161:112381.

[73] Sapp, M. (2022). World's first commercial scale co_2-to-methanol plant commissioned in china. https://www.biofuelsdigest.com/bdigest/2022/11/08/. Accessed on April 22, 2023.

[74] Sdanghi, G., Maranzana, G., Celzard, A., and Fierro, V. (2019). Review of the current technologies and performances of hydrogen compression for stationary and automotive applications. *Renewable and Sustainable Energy Reviews*, 102:150–170.

[75] Sherif, S. A., Goswami, D. Y., Stefanakos, E. L., and Steinfeld, A. (2014). *Handbook of hydrogen energy*. CRC press.

[76] Siemens Energy (2020). Hydrogen infrastructure – the pillar of energy transition. https://www.gascade.de/fileadmin/downloads/wasserstoff/. Accessed on January 27, 2023.

[77] Son, H., Yu, T., Hwang, J., and Lim, Y. (2022). Simulation methodology for hydrogen liquefaction process design considering hydrogen characteristics. *International Journal of Hydrogen Energy*, 47(61):25662–25678.

[78] Statista Research Department (2023). Global traded ammonia volume 2021-2050. https://www.statista.com/statistics/1345806/forecast-global-traded-ammonia-volume/. Accessed on March 23, 2023.

[79] The Royal Society (2020). Ammonia: zero-carbon fertiliser, fuel and energy store. https://royalsociety.org/topics-policy/projects/low-carbon-energy-programme/green-ammonia/. Accessed on March 07, 2023.

[80] Towler, G. and Sinnott, R. (2022). Chapter 7 - capital cost estimating. In *Chemical Engineering Design: Principles, Practice and Economics of Plant and Process Design*, pages 239–278. Butterworth-Heinemann, third edition.

[81] World, M. R. (2022). Liquid ammonia market 2022: Industry size, share, growth rate, sales ; revenue, key players, type and application, industry demand, trends and forecast to 2028: Research report by market reports world. https://www.globenewswire.com/news-release/2022/04/29/. Accessed on April 27, 2023.

[82] Yoon, M. (2020). Liquid-organic hydrogen carrier. https://encyclopedia.pub/entry/3331. Accessed: 2023-2-27.

[83] Zhang, C., Song, P., Zhang, Y., Xiao, L., Hou, J., and Wang, X. (2022). Technical and cost analysis of imported hydrogen based on mch-tol hydrogen storage technology. *International Journal of Hydrogen Energy*, 47(65):27717–27732.

A

MODEL ASSUMPTIONS AND DATA

Table A.1: General assumptions set -1

Electricity cost	0.04	€/kWh
Annual hours	8760.00	h
Truck speed	60.00	km/hr
fuel consumption truck	0.30	L/km
Diesel rate	1.19	€/L
Contingency	0.10	
Discount rate trucks	0.08	
lifetime	8.00	years
CRF	0.17	
TCI per truck	169270.00	€
OM truck	0.12	
OM trailers	0.02	
Trailer payload [66]		
GH_2 trailer	720.00	kg
LOHC trailer	4300.00	kg
LH_2 trailer	4500.00	kg
NH_3 trailer	20000.00	kg
Loading time		
GH_2 trailer	2.00	h
LOHC trailer	1.50	h
LH_2 trailer	3.00	h
NH_3 trailer	2.00	h

A

Table A.2: Trailer cost assumptions adjusted to 2022 price [37], [66]

TCI per trailer		
GH_2	581850	€
LH_2	717260	€
NH_3	122720	€
LOHC	158690	€

Table A.3: Densities of chemicals and oils

LH_2	71.00	kg/m^3
NH_3	681.66	kg/m^3
MeOH	792.00	kg/m^3
DBT	1040.00	kg/m^3
PDBT	910.00	kg/m^3
MCH	770.00	kg/m^3
Toluene	867.00	kg/m^3
HFO	1010.00	kg/m^3

Table A.4: Price assumptions for chemicals and oils

N_2	0.20	€/kg
Toluene	0.37	€/kg
DBT	4.93	€/kg
CO_2	0.10	€/kg
Helium	52.44	€/kg
NG	2.25	$€/m^3$
HFO	375.00	€/ton

Table A.5: Assumptions for storage systems [62], [66]

Storage duration	60.00	days
NH_3	0.95	€/kg
LOHC	236.72	$€/m^3$
LH_2	30.82	€/kg

Table A.6: Assumptions for ammonia ships [62]

Capacity MGC	35000.00	m^3
Capacity LGC	59000.00	m^3
Filling_limit	0.98	
loading_rate_MGC	1814000.00	kg/hr
loading_rate_LGC	2734000.00	kg/hr
charter_MGC	26628.00	€/day
charter_LGC	36614.00	€/day
speed_MGC	27.78	km/hr
speed_LGC	29.89	km/hr
Fuel consumption MGC	37.00	tons/day
Fuel consumption LGC	37.00	tons/day

Table A.7: Assumptions for LH_2 and LOHC ships

LH_2 ship		
LH_2	12658.00	kg
speed	33.34	km/hr
Fuel cons	9.26	L/km
Loading time	48.00	h
TCI LH_2 ship	146000000.00	€
Operating	11500.00	€/day
LOHC ships		
LOHC	52560.00	m^3
speed LOHC ship	27.70	km/hr
Fuel cons LOHC ship	9.58	L/km
TCI LOHC ship	35000000.00	€
Loading time	48.00	h
operating	5000.00	€/day

B

ECONOMIC ANALYSIS RESULTS

Cost estimation is based on the guidelines provided in the book "Chemical Engineering Design: Principles, Practice and Economics of Plant and Process Design" [80].

B

Table B.1: Hydrogen liquefaction economic analysis

Equipment	Tag	Sizing term	Sizing unit	Ce2022	TCI (USD 2022)
Reciprocating compressor		Driver power	kW		
	K-100	5735		2866355	16693652
	K-101	5851		2904199	16914055
	K-102	5852		2904524	16915950
Multistream HX		Area #	m^2		
	LNG100	6309.16		565206	3291760
	LNG103	2697.15		247349	1440561
	LNG102	98.76		18691	108856
S&T Heat exchanger		Area	m^2		0
	E100	847.19		860959	5014227
	E101	551.41		561794	3271887
	E103	844.37		857991	4996942
	E104	26.76		43273	252024
	E102	3.51		39696	231192
Separator		Shell mass	kg		
	V- CS				
	Separator	574.66		26892	156619
Expander		HP			
		839.60		88306	514294
		692.70		75567	440103
					70242123

The heat transfer area for multistream cryogenic heat exchangers is calculated based on the overall heat transfer coefficient of 0.5 $kW/m^2 \cdot K$ [15].

Table B.2: Ammonia synthesis economic analysis

Equipment	Tag	Sizing term	Sizing unit	Ce2022	TCI (USD 2022)
Reciprocating compressor		Driver power	kW		
	K-100	963.00		1021458	5948972
	K-101	989.40		1034901	6027262
	K102	391.00		699116	4071652
	K103	109.20		493628	2874890
Separator		Shell mass	kg		
	KOD-1	1495.67		40178	233997
	V1	568.97		26803	156099
	V2	568.97		26803	156099
S&T Heat exchanger		Area	m^2		
	E100	71.81		52168	303824
	E101	339.60		122033	710718
	E102	133.39		66293	386092
	E103	27.89		43473	253188
	E104	335.55		120851	703836
	E105	358.00		127437	742193
	E106	26.08		43155	251332
	E107	18.15		41814	243526
	E108	237.42		93163	542581
Reactor		volume	m^3		
	R100	3.93		222884	1298077
	R101	3.93		222884	1298077
	R102	3.93		222884	1298077
Total					27500494

B

Table B.3: Ammonia cracking economic analysis

Equipment	Tag	Sizing term	Sizing unit	Ce2022	TCI (USD 2022)
Pump		Flow	L/s		
	P-100	4.54		12561	73155
Shell and Tube					
	E100	25.12		42987	250358
	E101	128.84		65195	379694
	E103	112.56		61328	357176
	E104	12.01		40854	237932
	Reboiler	68.31		51422	299480
	Condenser	6.26		40040	233192
Fired Heaters		duty	MW		
	E102	2.45		426200	2482188
	For Reactor	8.97		998491	5815209
Reactor		volume	m^3		
		10.60		388410	2262097
Vessels	V- CS				
Absorber	T100	6304.93		97408	567305
Distillation column	T101	3265.00		62661	364938
Packings		Diameter	m		
Sieve tray		0.61		436	
				4801	27960
Pall rings		2.84		33980	197901
		10.60		388410	2262097
PSA	H2 (kg/hr)	nm^3/hr			
	1772.073903	19705.46			16797004#
Total					32607686

Cost relation for hydrogen production (nm^3/hr) and investment cost for PSA unit obtained from *Luo et al.* [55].

Table B.4: Methanol synthesis economic analysis

Equipment	Tag	Sizing term	Sizing unit	Ce2022	TCI (USD 2022)
Reciprocating compressor		Driver power	kW		
	K-100	183.80		554869	3231556
	K-101	693.20		878111	5114120
	K102	832.90		953796	5554909
Separator		Shell mass	kg		0
	KOD-1	848.00		31042	180791
	V1	1265.00		37010	215545
	V2	606.00		27381	159466
	DC	3654.03		67316	392048
				0	0
S&T Heat exchanger		Area	m^2	0	0
	E100	20.92		42271	246188
	E101	20.92		42271	246188
	E102	98.94		58177	338822
	E103	10.00		40557	236206
	E104	25.72		43092	250966
					0
Static mixer		Flowrate	L/s		0
	Mix-100	140.36		12684	73871
		316.00		17241	100411
Trays		Diameter	m		0
24		1.50		35179	204883
					0
Reactor		volume	m^3		0
	R100	3.93		222884	1298077
					0
Total					17844050

B

Table B.5: Methanol reforming economic analysis

Equipment	Tag	Sizing term	Sizing unit	Ce2022	TCI (USD 2022)
Static mixer		Flowrate	L/s		
	Mix-100	5		3871	22543
Pump		Flow	L/s		
	P-100	5		12618	73486
Heaters		Duty	MW		
	E100	7	MW	852871	4967123
	Reactor	5	MW	660064	3844213
Heat Exchangers					
	E101	55		48670	283451
	E102	91		56286	327808
Reactor		volume	m^3		
	R100	6		97176	565953
	kg/hr	nm^3/hr			
PSA	1792	19927			16910054#
Total					26994632

Cost relation for hydrogen production (nm^3/hr) and investment cost for PSA unit obtained from *Luo et al.* [55].

Table B.6: DBT Hydrogenation economic analysis

Equipment	Tag	Sizing term	Sizing unit	Ce2022	TCI (USD 2022)
Reciprocating compressor		Driver power	kW		
	K-100	363.20		681160	3967074
	K-101	371.90		686815	4000010
					0
Pump		Flow	L/s		0
	P-100	7.21		13240	77111
					0
Separator	V- CS	Shell mass	kg		0
					0
	KOD-1	1065.00		34192	199134
	Separator-1	590.00		27132	158015
					0
S&T Heat exchanger		Area	m^2		0
	E100	15.12		41331	240710
	E101	7.53		40210	234183
	E102	52.98		48249	281002
	E103	193.27		81392	474028
Reactor		volume	m^3		0
		5.04		86797	505509
					10136777

B

Table B.7: PDBT Dehydrogenation economic analysis

Equipment	Tag	Sizing term	Sizing unit	Ce2022	TCI (USD 2022)
Pump		Flow	L/s		
	P-100	8.24		13495	78596
Separator		Shell mass	kg		
	Separator-1	574.66		26892	156619
S&T Heat exchanger		Area	m^2		
	E100	36.66		45073	262503
	E102	110.69		60890	354622
Fired heater		Duty	MW		
	E101	2.95		476556	2775461
	For Reactor	5.81		738828	4302935
Reactor		volume	m^3		
		3.93		76067	443014
Total					8373751

Table B.8: Toluene hydrogenation economic analysis

Equipment	Tag	Sizing term	Sizing unit	Ce2022	TCI (USD 2022)
Pump		Flow	L/s		0
	P-100	8.75		13620	79324
Separator		Shell mass	kg		
	V- CS				
	Separator-1	590.00		27132	158015
S&T Heat exchanger		Area	m^2		
	E100	24.06		42804	249292
	E102	34.94		44752	260637
	E104			39354	
Fired heater	E101	2.01	MW	380140	2213937
	E103	1.19	MW	287925	1676877
Reactor		volume	m^3		
		3.93		222888	1298097
Total					5936179

B

Table B.9: MCH Dehydrogenation economic analysis

Equipment	Tag	Sizing term	Sizing unit	Ce2022	TCI (USD 2022)
Pumps		Flow	L/s		0
	P-100	10.41		14022	81666
Separator		Shell mass	kg		
	Separator-1	606.00		27381	159466
	Separator-2	575.00		26897	156650
S&T Heat exchangers		Area	m^2		
	E100	61.53		49999	291195
	E102	174.50		76541	445774
		Duty	MW		
Fired heater	E101	5.27	MW	691133	4025159
		16.02	MW	1521706	8862417
Chiller	E103	404.00		273328	1591862
Static mixer		Flowrate	L/s		
	Mix-100	8.30	2	4635	26995
Reactor		volume	m^3		
		3.93		222888	1298097
Total					16939282

C

SIMULATION STREAM PROPERTIES

C

Table C.1: Hydrogen liquefaction material stream properties

Name	Vapour Fraction	Temperature °C	Pressure [kPa]	Molar Flow [kgmole/h]	Mass Flow [kg/h]
1	1.00	30.00	3000.00	892.86	1800.00
2	1.00	-89.45	300.00	892.86	1800.00
3	1.00	-86.25	300.00	892.86	1800.00
4	1.00	-54.46	300.00	1042.04	2100.75
5	1.00	25.00	300.00	1042.04	2100.75
6	1.00	-190.00	300.00	1042.04	2100.75
7	0.78	-249.51	300.00	1042.04	2100.75
8	0.00	-249.60	300.00	1042.04	2100.75
9	0.14	-254.46	101.32	1042.04	2100.75
10	0.00	-254.46	101.32	892.48	1799.24
11	1.00	-254.46	101.32	149.56	301.52
12	1.00	-252.00	101.32	149.56	301.52
13	1.00	-194.30	101.32	149.56	301.52
14	1.00	24.00	101.32	149.56	301.52
15	1.00	5.00	101.32	149.56	301.52
16	1.00	134.46	300.00	149.56	301.52
17	1.00	134.46	300.00	149.18	300.75
18	1.00	24.00	101.32	9992.55	40000.00
19	1.00	123.34	183.32	9992.55	40000.00
20	1.00	30.00	183.32	9992.55	40000.00
21	1.00	131.35	331.66	9992.55	40000.00
22	1.00	30.00	331.66	9992.55	40000.00
23	1.00	131.36	600.03	9992.55	40000.00
24	1.00	25.00	600.03	9992.55	40000.00
25	1.00	-190.00	600.03	9992.55	40000.00
26	1.00	-242.50	600.03	9992.55	40000.00
27	1.00	-255.23	101.32	9992.55	40000.00
28	1.00	-252.00	101.32	9992.55	40000.00
29	1.00	-190.56	101.32	9992.55	40000.00
30	0.00	-196.00	101.32	467.61	13099.18
31	1.00	24.00	101.32	467.61	13099.18

Table C.2: Hydrogen liquefaction stream compositions

Name	H_2	H_2O	N_2	He
1	1.00	0.00	0.00	0.00
2	1.00	0.00	0.00	0.00
3	1.00	0.00	0.00	0.00
4	1.00	0.00	0.00	0.00
5	1.00	0.00	0.00	0.00
6	1.00	0.00	0.00	0.00
7	1.00	0.00	0.00	0.00
8	1.00	0.00	0.00	0.00
9	1.00	0.00	0.00	0.00
10	1.00	0.00	0.00	0.00
11	1.00	0.00	0.00	0.00
12	1.00	0.00	0.00	0.00
13	1.00	0.00	0.00	0.00
14	1.00	0.00	0.00	0.00
15	1.00	0.00	0.00	0.00
16	1.00	0.00	0.00	0.00
17	1.00	0.00	0.00	0.00
18	0.00	0.00	0.00	1.00
19	0.00	0.00	0.00	1.00
20	0.00	0.00	0.00	1.00
21	0.00	0.00	0.00	1.00
22	0.00	0.00	0.00	1.00
23	0.00	0.00	0.00	1.00
24	0.00	0.00	0.00	1.00
25	0.00	0.00	0.00	1.00
26	0.00	0.00	0.00	1.00
27	0.00	0.00	0.00	1.00
28	0.00	0.00	0.00	1.00
29	0.00	0.00	0.00	1.00
30	0.00	0.00	1.00	0.00
31	0.00	0.00	1.00	0.00

C

Table C.3: Ammonia synthesis material stream properties

Name	Vapour fraction	Temperature °C	Pressure (kPa)	Molar flow (kmole/h)	Mass flow (kg/h)
1	1.00	35.00	3000.00	888.00	1790.21
2	1.00	30.00	3000.00	296.00	8291.85
3	1.00	33.06	3000.00	1184.00	10082.06
4	1.00	133.74	6708.00	1184.00	10082.06
5	1.00	35.00	6708.00	1184.00	10082.06
6	1.00	136.68	14999.09	1184.00	10082.06
7	1.00	42.90	14999.09	10438.34	92600.01
8	1.00	310.12	14999.09	10438.34	92600.01
9	1.00	331.63	14999.09	10438.34	92600.01
10	1.00	400.00	14999.09	10438.34	92600.01
11	0.00	468.75	14999.09	0.00	0.00
12	1.00	468.75	14999.09	10024.06	92599.81
13	1.00	400.00	14999.09	10024.06	92599.81
14	0.00	421.70	14999.09	0.00	0.00
15	1.00	421.70	14999.09	9894.51	92599.74
16	1.00	400.00	14999.09	9894.51	92599.74
17	0.00	407.55	14999.09	0.00	0.00
18	1.00	407.55	14999.09	9849.59	92599.72
19	1.00	134.59	14999.09	9849.81	92589.28
20	1.00	35.00	14999.09	9849.81	92589.28
21	0.98	16.11	14999.09	9849.81	92589.28
22	0.96	6.00	14999.09	9849.81	92589.28
23	0.94	-2.70	14999.09	9849.81	92589.28
24	1.00	-2.70	14999.09	9254.34	82517.96
25	1.00	30.00	14999.09	9254.34	82517.96
26	1.00	29.95	14819.09	9254.34	82517.96
27	1.00	31.36	15000.00	9254.34	82517.96
28	1.00	31.36	15000.00	9254.34	82517.96
29	0.00	-2.70	14999.09	595.47	10071.32
30	0.01	0.13	2000.00	595.47	10071.32
31	1.00	0.13	2000.00	7.64	70.12
32	0.00	0.13	2000.00	587.83	10001.20
33	0.02	-3.88	400.00	587.83	10001.20
34	0.46	-1.66	400.00	587.83	10001.20
35	1.00	-1.66	400.00	269.53	4580.52
36	1.00	150.83	2000.00	269.53	4580.52
37	0.01	35.00	2000.00	269.53	4580.52
38	0.00	-1.66	400.00	318.30	5420.68
39	0.00	-1.20	2000.00	318.30	5420.68

Table C.4: Ammonia synthesis material stream properties

Name	Vapour fraction	Temperature °C	Pressure (kPa)	Molar flow (kmole/h)	Mass flow (kg/h)
CW1	0.00	30.00	700.00	2948.51	53117.66
CW2	0.00	45.00	700.00	2948.51	53117.66
CW3	0.00	30.00	700.00	26743.40	481785.02
CW4	0.00	45.00	700.00	26743.40	481785.02
CW7	0.00	30.00	700.00	5579.92	100522.87
CW8	0.00	45.00	700.00	5579.92	100522.87
Refrigerant 1	0.00	-196.00	101.32	686.01	19217.10
Refrigerant 2	1.00	2.00	101.32	686.01	19217.10

Table C.5: Ammonia synthesis stream compositions

Name	H_2	H_2O	N_2	NH_3
CW1	0.00	1.00	0.00	0.00
CW2	0.00	1.00	0.00	0.00
CW3	0.00	1.00	0.00	0.00
CW4	0.00	1.00	0.00	0.00
CW7	0.00	1.00	0.00	0.00
CW8	0.00	1.00	0.00	0.00
Refrigerant 1	0.00	0.00	1.00	0.00
Refrigerant 2	0.00	0.00	1.00	0.00

Table C.6: Ammonia synthesis stream compositions

Name	H_2	H_2O	N_2	NH_3
1	1.00	0.00	0.00	0.00
2	0.00	0.00	1.00	0.00
3	0.75	0.00	0.25	0.00
4	0.75	0.00	0.25	0.00
5	0.75	0.00	0.25	0.00
6	0.75	0.00	0.25	0.00
7	0.72	0.00	0.24	0.04
8	0.72	0.00	0.24	0.04
9	0.72	0.00	0.24	0.04
10	0.72	0.00	0.24	0.04
11	0.69	0.00	0.23	0.08
12	0.69	0.00	0.23	0.08
13	0.69	0.00	0.23	0.08
14	0.68	0.00	0.23	0.10
15	0.68	0.00	0.23	0.10
16	0.68	0.00	0.23	0.10
17	0.67	0.00	0.22	0.10
18	0.67	0.00	0.22	0.10
19	0.67	0.00	0.22	0.10
20	0.67	0.00	0.22	0.10
21	0.67	0.00	0.22	0.10
22	0.67	0.00	0.22	0.10
23	0.67	0.00	0.22	0.10
24	0.71	0.00	0.24	0.05
25	0.71	0.00	0.24	0.05
26	0.71	0.00	0.24	0.05
27	0.71	0.00	0.24	0.05
28	0.71	0.00	0.24	0.05
29	0.01	0.00	0.00	0.99
30	0.01	0.00	0.00	0.99
31	0.63	0.00	0.14	0.23
32	0.00	0.00	0.00	1.00
33	0.00	0.00	0.00	1.00
34	0.00	0.00	0.00	1.00
35	0.00	0.00	0.00	1.00
36	0.00	0.00	0.00	1.00
37	0.00	0.00	0.00	1.00
38	0.00	0.00	0.00	1.00
39	0.00	0.00	0.00	1.00

Table C.7: Ammonia cracking material stream properties

Name	Vapour Fraction	Temperature °C	Pressure [kPa]	Molar Flow [kgmole/h]	Mass Flow [kg/h]
1	0.00	-33.00	101.32	587.80	10010.23
2	0.00	-32.81	1000.00	587.80	10010.23
3	0.00	-32.00	1000.00	602.80	10265.67
4	1.00	24.22	970.00	602.80	10265.67
6	1.00	700.00	910.00	602.80	10265.67
7	1.00	700.00	910.00	1188.81	10266.02
5	1.00	418.00	940.00	602.80	10265.67
8	1.00	423.50	880.00	1188.81	10266.02
9	1.00	35.00	850.00	1188.81	10266.02
10	1.00	15.00	850.00	1188.81	10266.02
11	0.00	15.00	600.00	166.53	3000.00
12	1.00	22.69	600.00	1178.53	10096.45
13	1.00	27.60	600.00	879.00	1772.07
14	0.99	27.60	600.00	299.53	8324.38
15	0.00	15.47	850.00	176.80	3169.57
16	0.00	157.53	600.00	161.80	2914.17
17	0.00	-1.49	500.00	15.00	255.40
18	0.00	-1.44	500.00	15.00	255.43
19	0.00	-1.30	1000.00	15.00	255.43
CW1	0.00	45.00	700.00	12971.93	233690.60
CW2	0.00	30.00	670.00	12971.93	233690.60
CW3	0.00	43.52	640.00	12971.93	233690.60

C

Table C.8: Ammonia cracking stream compositions

Name	N_2	H_2	H_2O	NH_3
1	0.00	0.00	0.00	1.00
2	0.00	0.00	0.00	1.00
3	0.00	0.00	0.00	1.00
4	0.00	0.00	0.00	1.00
5	0.00	0.00	0.00	1.00
6	0.00	0.00	0.00	1.00
7	0.25	0.74	0.00	0.01
8	0.25	0.74	0.00	0.01
9	0.25	0.74	0.00	0.01
10	0.25	0.74	0.00	0.01
11	0.00	0.00	1.00	0.00
12	0.25	0.75	0.00	0.00
13	0.00	1.00	0.00	0.00
14	0.98	0.00	0.02	0.00
15	0.00	0.00	0.91	0.09
16	0.00	0.00	1.00	0.00
17	0.00	0.00	0.00	1.00
18	0.00	0.00	0.00	1.00
19	0.00	0.00	0.00	1.00
CW1	0.00	0.00	1.00	0.00
CW2	0.00	0.00	1.00	0.00
CW3	0.00	0.00	1.00	0.00

Table C.9: MeOH synthesis material stream properties

Name	Vapour fraction	Temperature °C	Pressure (kPa)	Molar flow (kmole/h)	Mass flow (kg/h)
1	1.00	35.00	1500.00	300.00	13202.91
2	1.00	97.82	3000.00	300.00	13202.91
3	1.00	35.00	2970.00	300.00	13202.91
4	0.00	35.00	2970.00	0.00	0.00
5	1.00	35.00	2970.00	300.00	13202.91
6	1.00	35.00	3000.00	900.00	1814.40
7	1.00	28.53	2970.00	1200.00	15017.31
8	1.00	95.57	5470.00	1200.00	15017.31
10	1.00	210.00	5440.00	39902.81	96340.97
11	0.00	225.08	5440.00	0.00	0.00
12	1.00	225.08	5440.00	39304.03	96340.76
13	0.99	65.01	5410.00	39304.03	96340.76
14	0.99	64.50	5380.00	39304.03	96340.76
15	0.98	35.00	5350.00	39304.03	96340.76
16	0.00	35.00	5350.00	600.10	14995.85
18	0.00	36.54	180.00	599.22	14992.16
19	0.00	50.00	150.00	599.22	14992.16
20	0.00	70.00	120.00	599.22	14992.16
21	0.00	104.54	120.00	302.93	5499.14
22	0.00	55.27	120.00	296.30	9493.03
23	0.00	35.00	101.32	296.30	9493.03
24	1.00	35.00	5350.00	38703.92	81344.91
25	1.00	37.68	5470.00	38703.92	81344.91
26	1.00	37.68	5470.00	38702.81	81323.66
CW1	0.00	30.00	600.00	745.87	13437.00
CW2	0.00	45.00	570.00	745.87	13437.00
CW3	0.00	30.00	600.00	38680.60	696834.85
CW4	0.00	45.00	570.00	38680.60	696834.85
CW5	0.00	30.00	600.00	447.52	8062.20
CW6	0.00	49.83	570.00	447.52	8062.20
Vent	1.00	36.54	180.00	0.88	3.68

Table C.10: MeOH synthesis stream compositions

Name	CO_2	CO	H_2	MeOH	H_2O
1	1.00	0.00	0.00	0.00	0.00
2	1.00	0.00	0.00	0.00	0.00
3	1.00	0.00	0.00	0.00	0.00
4	1.00	0.00	0.00	0.00	0.00
5	1.00	0.00	0.00	0.00	0.00
6	0.00	0.00	1.00	0.00	0.00
7	0.25	0.00	0.75	0.00	0.00
8	0.25	0.00	0.75	0.00	0.00
10	0.01	0.00	0.99	0.00	0.00
11	0.00	0.00	0.98	0.01	0.01
12	0.00	0.00	0.98	0.01	0.01
13	0.00	0.00	0.98	0.01	0.01
14	0.00	0.00	0.98	0.01	0.01
15	0.00	0.00	0.98	0.01	0.01
16	0.00	0.00	0.00	0.50	0.50
18	0.00	0.00	0.00	0.50	0.50
19	0.00	0.00	0.00	0.50	0.50
20	0.00	0.00	0.00	0.50	0.50
21	0.00	0.00	0.00	0.01	0.99
22	0.00	0.00	0.00	1.00	0.00
23	0.00	0.00	0.00	1.00	0.00
24	0.00	0.00	1.00	0.00	0.00
25	0.00	0.00	1.00	0.00	0.00
26	0.00	0.00	1.00	0.00	0.00
CW1	0.00	0.00	0.00	0.00	1.00
CW2	0.00	0.00	0.00	0.00	1.00
CW3	0.00	0.00	0.00	0.00	1.00
CW4	0.00	0.00	0.00	0.00	1.00
CW5	0.00	0.00	0.00	0.00	1.00
CW6	0.00	0.00	0.00	0.00	1.00
Vent	0.00	0.00	0.92	0.06	0.01

Table C.11: MeOH reforming material stream properties

Name	Vapour Fraction	Temperature (°C)	Pressure (kPa)	Molar Flow (kgmole/h)	Mass Flow (kg/h)
1	0.00	25.00	101.32	296.27	9493.00
2	0.00	25.00	101.32	296.27	5337.30
3	0.00	39.89	101.32	592.54	14830.30
4	0.00	40.02	1060.00	592.54	14830.30
5	0.00	119.00	1030.00	592.54	14830.30
6	1.00	250.00	1000.00	592.54	14830.30
7	1.00	250.00	1000.00	1185.08	14830.58
8	1.00	125.78	970.00	1185.08	14830.58
9	1.00	35.00	940.00	1185.08	14830.58
10	1.00	36.76	940.00	888.81	1791.84
11	1.00	36.77	940.00	296.27	13038.74
CW1	0.00	30.00	700.00	2917.64	52561.60
CW2	0.00	45.00	670.00	2917.64	52561.60

Table C.12: MeOH reforming stream compositions

Name	MeOH	H_2	H_2O	CO	CO_2
1	1.00	0.00	0.00	0.00	0.00
2	0.00	0.00	1.00	0.00	0.00
3	0.50	0.00	0.50	0.00	0.00
4	0.50	0.00	0.50	0.00	0.00
5	0.50	0.00	0.50	0.00	0.00
6	0.50	0.00	0.50	0.00	0.00
7	0.00	0.75	0.00	0.00	0.25
8	0.00	0.75	0.00	0.00	0.25
9	0.00	0.75	0.00	0.00	0.25
10	0.00	1.00	0.00	0.00	0.00
11	0.00	0.00	0.00	0.00	1.00
CW1	0.00	0.00	1.00	0.00	0.00
CW2	0.00	0.00	1.00	0.00	0.00

C

Table C.13: DBT hydrogenation material stream properties

Name	Vapour fraction	Temperature °C	Pressure (kPa)	Molar flow (kmole/h)	Mass flow (kg/h)
1	0.00	30.00	101.32	99.21	27023.76
2	0.00	30.21	7050.00	99.21	27023.76
3	0.00	170.00	7020.00	99.21	27023.76
4	1.00	30.00	3000.00	892.14	1798.55
5	1.00	80.95	4615.20	892.14	1798.55
6	1.00	35.00	4585.20	892.14	1798.55
7	0.00	35.00	4585.20	0.00	0.00
8	1.00	35.00	4585.20	892.14	1798.55
9	1.00	86.85	7053.87	892.14	1798.55
10	1.00	170.00	7023.87	892.14	1798.55
13	1.00	491.17	7020.00	0.00	0.00
14	0.00	491.17	7020.00	107.36	28821.91
15	1.00	440.54	191.30	107.36	28821.91
16	1.00	414.38	161.30	107.36	28821.91
17	0.61	359.08	131.30	107.36	28821.91
18	0.08	35.00	101.32	107.36	28821.91
19	0.00	35.00	101.32	99.28	28805.63
20	1.00	35.00	101.32	8.08	16.28
CW1	0.00	30.00	700.00	1011.18	18216.46
CW2	0.00	45.00	670.00	1011.18	18216.46
CW3	0.00	30.00	700.00	22114.24	398390.17
CW4	0.00	45.00	670.00	22114.24	398390.17

Table C.14: DBT hydrogenation stream compositions

Name	H_2	H_2O	DBT	PDBT
1	0.00	0.00	1.00	0.00
2	0.00	0.00	1.00	0.00
3	0.00	0.00	1.00	0.00
4	1.00	0.00	0.00	0.00
5	1.00	0.00	0.00	0.00
6	1.00	0.00	0.00	0.00
7	1.00	0.00	0.00	0.00
8	1.00	0.00	0.00	0.00
9	1.00	0.00	0.00	0.00
10	1.00	0.00	0.00	0.00
13	0.08	0.00	0.01	0.91
14	0.08	0.00	0.01	0.91
15	0.08	0.00	0.01	0.91
16	0.08	0.00	0.01	0.91
17	0.08	0.00	0.01	0.91
18	0.08	0.00	0.01	0.91
19	0.00	0.00	0.01	0.99
20	1.00	0.00	0.00	0.00
CW1	0.00	1.00	0.00	0.00
CW2	0.00	1.00	0.00	0.00
CW3	0.00	1.00	0.00	0.00
CW4	0.00	1.00	0.00	0.00

Table C.15: PDBT dehydrogenation material stream properties

Name	Vapour fraction	Temperature °C	Pressure (kPa)	Molar flow (kmole/h)	Mass flow (kg/h)
1	0.00	30.00	101.32	98.22	28535.25
2	0.00	30.02	230.00	98.22	28535.25
3	0.00	127.00	200.00	98.22	28535.25
4	0.00	280.00	170.00	98.22	28535.25
5	0.90	200.00	170.00	974.73	28535.72
6	0.90	133.99	140.00	974.73	28535.72
7	0.90	35.00	101.32	974.73	28535.72
8	1.00	35.00	101.32	876.46	1766.94
9	0.00	35.00	101.32	98.27	26768.78
CW1	0.00	30.00	700.00	6093.98	109783.60
CW2	0.00	45.00	670.00	6093.98	109783.60

C

Table C.16: PDBT dehydrogenation stream compositions

Name	H_2	H_2O	DBT	PDBT
1	0.00	0.00	0.00	1.00
2	0.00	0.00	0.00	1.00
3	0.00	0.00	0.00	1.00
4	0.00	0.00	0.00	1.00
5	0.90	0.00	0.10	0.00
6	0.90	0.00	0.10	0.00
7	0.90	0.00	0.10	0.00
8	1.00	0.00	0.00	0.00
9	0.00	0.00	0.99	0.01
CW1	0.00	1.00	0.00	0.00
CW2	0.00	1.00	0.00	0.00

Table C.17: Toluene hydrogenation material stream properties

Name	Vapour fraction	Temperature °C	Pressure (kPa)	Molar flow (kmole/h)	Mass flow (kg/h)
1	1.00	35.00	860.00	892.86	1800.00
2	1.00	185.00	830.00	892.86	1800.00
3	0.00	30.00	101.32	297.61	27422.00
4	0.00	30.29	890.00	297.61	27422.00
5	0.09	207.66	860.00	297.61	27422.00
6	1.00	207.70	830.00	297.61	27422.00
7	1.00	194.15	830.00	1190.47	29222.00
8	1.00	250.00	800.00	1190.47	29222.00
9	0.00	350.00	800.00	0.00	0.00
10	1.00	350.00	800.00	306.57	29222.06
11	1.00	215.00	770.00	306.57	29222.06
12	0.74	188.03	740.00	306.57	29222.06
13	1.00	147.49	131.33	306.57	29222.06
14	0.03	30.00	101.33	306.57	29222.06
15	1.00	30.00	101.33	9.61	96.08
16	0.00	30.00	101.33	296.95	29125.98
CW1	0.00	25.00	700.00	10217.89	184076.27
CW2	0.00	45.00	670.00	10217.89	184076.27

Table C.18: Toluene hydrogenation stream compositions

Name	Toluene	H_2	H_2O	MCH
1	0.00	1.00	0.00	0.00
2	0.00	1.00	0.00	0.00
3	1.00	0.00	0.00	0.00
4	1.00	0.00	0.00	0.00
5	1.00	0.00	0.00	0.00
6	1.00	0.00	0.00	0.00
7	0.25	0.75	0.00	0.00
8	0.25	0.75	0.00	0.00
9	0.01	0.03	0.00	0.96
10	0.01	0.03	0.00	0.96
11	0.01	0.03	0.00	0.96
12	0.01	0.03	0.00	0.96
13	0.01	0.03	0.00	0.96
14	0.01	0.03	0.00	0.96
15	0.00	0.92	0.00	0.08
16	0.01	0.00	0.00	0.99
CW1	0.00	0.00	1.00	0.00
CW2	0.00	0.00	1.00	0.00

Table C.19: MCH dehydrogenation material stream properties

Name	Vapour fraction	Temperature °C	Pressure (kPa)	Molar flow (kmole/h)	Mass flow (kg/h)
1	0.00	20.00	101.32	293.84	28851.97
2	0.00	20.06	240.00	293.84	28851.97
4	1.00	360.00	210.00	293.84	28851.97
6	1.00	300.00	210.00	1166.55	28851.91
5	0.00	300.00	210.00	0.00	0.00
7	1.00	135.00	180.00	1166.55	28851.91
3	0.68	128.86	210.00	293.84	28851.97
8	0.78	30.00	150.00	1166.55	28851.91
9	1.00	30.00	150.00	904.62	4715.24
14	0.00	30.00	150.00	261.93	24136.67
10	1.00	29.98	101.32	904.62	4715.24
11	0.98	5.00	101.32	904.62	4715.24
12	1.00	5.00	101.32	884.82	2889.52
13	0.00	5.00	101.32	19.80	1825.72
15	0.00	28.33	101.32	281.73	25962.40
CW1	0.00	30.00	700.00	13777.59	248204.68
CW2	0.00	45.00	670.00	13777.59	248204.68

C

Table C.20: MCH dehydrogenation stream compositions

Name	Toluene	H_2O	H_2	MCH
1	0.00	0.00	0.00	1.00
2	0.00	0.00	0.00	1.00
4	0.00	0.00	0.00	1.00
6	0.25	0.00	0.75	0.00
5	0.25	0.00	0.75	0.00
7	0.25	0.00	0.75	0.00
3	0.00	0.00	0.00	1.00
8	0.25	0.00	0.75	0.00
9	0.03	0.00	0.96	0.00
14	0.99	0.00	0.00	0.01
10	0.03	0.00	0.96	0.00
11	0.03	0.00	0.96	0.00
12	0.01	0.00	0.99	0.00
13	0.99	0.00	0.00	0.01
15	0.99	0.00	0.00	0.01
CW1	0.00	1.00	0.00	0.00
CW2	0.00	1.00	0.00	0.00